Key Engineering Materials Vols. 373-374
(July 2008)

Surface Engineering

Edited by
M.K. Lei, X.P. Zhu,
K.W. Xu and B.S. Xu

TRANS TECH PUBLICATIONS

Surface Engineering

Surface Engineering

Selected, peer reviewed papers from the Fifth International Conference on Surface Engineering (ICSE 2007)

Edited by

M.K. Lei and X.P. Zhu

Dalian University of Technology, China

K.W. Xu

Xi'an Jiaotong University, China

B.S. Xu

National Key Laboratory for Remanufacturing, China

TRANS TECH PUBLICATIONS LTD

Switzerland • UK • USA

Trans Tech Publications Ltd
Laubisrutistr. 24
CH-8712 Stafa-Zurich
Switzerland
http://www.ttp.net

Volumes 373-374- of
Key Engineering Materials
ISSN 1013-9826
Full text available online at *http://www.scientific.net*

Distributed *worldwide by*

Trans Tech Publications Ltd.
Laubisrutistr. 24
CH-8712 Stafa-Zurich
Switzerland

Fax: +41 (44) 922 10 33
e-mail: sales@ttp.net

and in the Americas by

Trans Tech Publications Inc.
PO Box 699, May Street
Enfield, NH 03748
USA

Phone: +1 (603) 632-7377
Fax: +1 (603) 632-5611
e-mail: sales-usa@ttp.net

Printed in the Netherlands

Committees

Chair and Co-chair of Conference
Chair: B.S. Xu (China)
Co-chair: T. Bell (UK)

Secretary-general: M.K. Lei (China)
Associate secretaries-general: F. Zhang (China) X.P. Zhu (China)

Consultant Committee
C.X. Ding (China) L.S. Wen (China) L. Zhou (China) Q.J. Xue (China)
Y.B. Xie (China) L.D. Wang (China) J.J. Liu (China) P.F. Ding (China)
M. Li (China) D.M. Guo (China) H. Michel (France) J.J. Moore (US)
E.P. Volchkov (Russia) I. Petrov (US) L. Vincent (France)
W. Wlosinski (Poland)

Academic Committee
Director: B.S. Xu (China)
Associate director: K.W. Xu (China)
Members: W. Chen (Canada) H. Dong (UK) S.Y. Ge (China)
S.C. Kwon (Korea) C.J. Li (China) A. Lin (China) X.Y. Liu (China)
J.B. Luo (China) S.N. Ma (China) E. Meletis (US) P.X. Qiao (China)
G.E. Remnev (Russia) M.A.J. Somers (Denmark) D.B. Sun (China)
F.H. Wang (China) G.B. Wang (China) H.G. Wang (China)
W. Wang (China) R. Wei (US) Z. Xu (China) L. Yan (China)
Q.F. Zhang (China) Z.R. Zhou (China) S. Zhu (China)

Organization Committee
Director: K.W. Xu (China)
Associate director: P.X. Qiao (China)
Members: Y.Y. Fan (China) H. Gao (China) Y.Z. Lei (China) J. Li (China)
L. Lin (China) X.X. Ma (China) X. Peng (China) X.H. Tong (China)
H.D. Wang (China) L. Wang (China) X.C. Wu (China) L. Xu (China)
D.F. Xue (China) Z.J. Zhang (China) M.H. Zhu (China) D.M. Zhuang (China)

Preface

The 5th International Conference on Surface Engineering (ICSE 2007) was held at Dalian University of Technology in Dalian, a beautiful coastal Chinese city, from July 7 to 10, 2007. Since 1997, its 1st to 4th meeting has been held periodically every 2-3 years, in Shanghai (1997), Wuhan (1999), Chengdu (2002) and Shenzhen (2004), respectively. The theme of ICSE 2007 is "Innovation and Development of Surface Engineering toward A Conservation-minded Society", timely reflecting the obligation of advanced technologies to energy & resource saving and environment protection for the world.

This conference is a grand gathering of the surface engineering community, which provided an active forum for specialists, scholars and engineers coming from the forefront of scientific research, teaching and industries worldwide to exchange their new ideas and discuss the latest developments in the commonly interested fields. Around 260 abstracts have been selected from more than 800 abstracts submitted, for presentation in the conference. Finally, nearly 300 delegates attended the conference, which include over 40 foreign delegates from UK, US, France, Japan, Korea, Germany, Sweden, and Netherlands etc. 100 oral presentations, including 2 plenary lectures and 13 invited talks, have been given on 7 special topics, namely thermal spraying technology, vapor deposition technology, electrodeposition and electroless deposition, energetic beams and plasma surface treatments, wear and corrosion behaviors of engineering surfaces, functional films and coatings, surface machining and mechanical processing technologies. From the submitted 260 manuscripts, 201 papers have been chosen for publication in this proceeding by peer reviewing process.

I believe that surface engineering must play a more and more important role in energy-saving, materials-saving and environment-protection in the coming years, to realize 4R (Reuse, Reduce, Recycle, Remanufacture) and contribute to world economy development.

I am grateful to the valuable financial support of National Natural Science Foundation of China, Dalian Association for Science and Technology, and Dalian University of Technology, to the highly effective preparation and the hard work of organizers. Finally, I give the great appreciation to all the authors, referees, the members of ICSE 2007 committees and the publisher Trans Tech Publications who have made the publication of this special volume possible through their efforts and kind cooperation.

Sincerely,

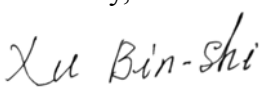

Bin-shi Xu
Chairman of ICSE 2007
Academician of Chinese Academy of Engineering
Director of National Key Laboratory for Remanufacturing
Bejing, 100072, China
December 8, 2007

Table of Contents

Committee

Preface

I. Thermal Spray Technology

The Remanufacturing Engineering and Automatic Surface Engineering Technology
B.S. Xu 1

Effect of Plasma Sprayed Ceramic and Cermet Coatings on Wear-Out Failure of High Temperature Ball Valve
L. Liu, B.Q. Gu and Y. Chen 11

Preparation and Characterization of Ni-Al-Cr_3C_2 Coating
L.Z. Du, W.G. Zhang, D.J. Zhang and B.H. Li 15

Comparative Study of 321 Stainless Steel and 321-Al Composite Coatings Deposited by Arc Spraying Process
Y.X. Chen, B.S. Xu, X.B. Liang and Y. Xu 19

Effect of HVOF Sprayed MCrAlY Coating on Thermomechanical and Isothermal Fatigue Life of Superalloy M963
Z.W. Huang, Z.G. Wang, S.J. Zhu, F.H. Yuan and F.G. Wang 23

Performance Study of Erosion Wear of Nanostructured WC-12Co Coatings Sprayed by HVOF
Z.X. Ding, Q. Wang and Z.L. Liu 27

Fabrication and Evaluation of Plasma-Sprayed Functionally Gradient W/Cu Coatings as Plasma Facing Materials in Fusion Devices
S.X. Song, W.Z. Yao, Z.J. Zhou, W.W. Cong, Y. Ma and C.C. Ge 31

Microstructure and Abrasion Resistance Mechanism of CrB Particles Reinforced MMC Coating
H.L. Deng, G.L. Li, Y.J. Song and S.R. Xiao 35

Micro-Damage Evolution and Residual Stress in Thermally Grown Oxides of Detonation Gun Sprayed Thermal Barrier Coatings
Z.X. Chen, S.J. Zhu, Z.G. Wang and F.H. Yuan 39

Plasma Transferred Arc Powder Surfacing Technology of Thrust Face
Y.H. Lv, B.S. Xu, Y.H. Xiang, D. Xia and C.L. Liu 43

Microstructure and Performance Analysis of Cr_3C_2-25%NiCr Coating Prepared by Plasma Spraying Process
C.M. Wang, H.F. Sun and Q. Song 47

Microstructure and Properties of Multi-Function Micro-Plasma Sprayed Al_2O_3 Coatings
S.C. Hua, H.G. Wang, L.Y. Wang and G. Liu 51

Effect of Heat Treatment on Microstructures and Properties of Zinc-Aluminum Coating on AZ91D Magnesium Alloy
J. Zhang and Y. Wang 55

Properties of Multi-Function Micro-Plasma Sprayed Nanostructured Al_2O_3-13wt%TiO_2 Coatings
L.Y. Wang, G. Liu, H.G. Wang and S.C. Hua 59

Corrosion Protection of A3 Steel with Zn-Al-Mg-RE Coating from Arc Spraying
Y. Liu, Y.X. Chen, J.Y. Bai, Z.X. Zhu, S.C. Wei, X.B. Liang and B.S. Xu 64

Influence of Substrate Temperature on Microcracks Formation in Plasma-Sprayed Yttria-Stabilized Zirconia Splats
Y.Z. Xing, Y. Li, C.J. Li, C.X. Li and G.J. Yang 69

Effect of Annealing Treatment on the Structure and Microhardness of Cold-Sprayed Nanostructured FeAl/WC Composite Coating
H.T. Wang, G.J. Yang, C.J. Li and C.X. Li 73

Study on Arc Spraying Technique for Repairing Automobile Parts Based on Four Factors Experimental Method
L.G. Liu 77

Study on the Plasma-Sprayed Molybdenum as Plasma Facing Materials in Fusion Reactor
W.Z. Yao, S.X. Song, Z.J. Zhou, W.W. Cong, Y. Ma and C.C. Ge 81

High Velocity Arc-Sprayed Coating by CrB Powder Wire for Elevated Temperature Erosion Protection in Circulating Fluidized Bed Boilers
Y.J. Song, H.L. Deng, S.R. Xiao and W.H. Shi 85

An Automatic High Velocity Arc Spraying System
J.Y. Bai, Y.X. Chen, J.B. Cheng, X.B. Liang and B.S. Xu 89

II. Vapour Deposition Technology

PVD-PECVD Hybrid Processes: Synthesis of Composite Thin Films and Process Understanding
T. Belmonte, A. Daniel and T. Duguet 93

RIBAD Deposition of TiN on Magnesium Alloy
S. Abela and M. Grech 100

Evolution of Nanoindentation Hardness of Fe/Cu Nanometer-Scale Multilayers by Magnetron Sputtering
J. Gao, Z.L. Wu, Z.P. Zhang, B.S. Cao and M.K. Lei 104

Molecular Dynamics Studies on the Growth and Structural Properties of Hydrogenated DLC Films
Y.J. Zhang, G.N. Dong, J.H. Mao and Y.B. Xie 108

Structure of Alumina Layer on the Damage Resistance of Multilayered CVD Coating under Repeated Impact Loading
X.D. Zhu, H.L. Dou, Z.G. Ban, Y.X. Liu and J.W. He 113

Study on the Mechanic Properties of DLC Films on Different Metal Substrates
D.C. Zhao, N. Ren, Z.J. Ma, G.J. Xiao and S.H. Wu 117

Material Design of Transition Metal Nitrides for Hard Coatings by Metal and Nonmetal Atom Substitution
T. Suzuki, J. Inoue, H. Asami, T. Ibi, T. Nakayama, H. Suematsu and K. Niihara 122

Synthesis and Characterization of CrXN Nano-Multilayer Coatings
H.Q. Li, X.Y. Li, H.L. Sun, D. Teer and H.S. Dong 126

Deposition of CrN Coatings by Filtered Cathodic Vacuum Arc
J.L. Mo, M.H. Zhu, J. An, H. Sun, Y.X. Leng and N. Huang 130

Polycrystalline Columnar Diamond Film Deposited on Spherical Substrate by DC Arc Plasma CVD
D.S. Li, D.W. Zuo, W.Z. Lu, R.F. Chen, B.K. Xiang and M. Wang 134

The Influence of the Magnetic Field Arrangement on the Titanium Oxide Films Properties for Four Targets Closed-Filed Unbalance Magnetron Sputtering
F. Qi, Y.X. Leng, H. Sun and N. Huang 138

Fabrication Of Nd:YVO_4 Thin Film Waveguide Grown on Si/SiO_2 by Pulsed Laser Deposition
H.X. Li, R.G. Song, X. Wu and J.Y. Wang 142

The Preparation and Properties of TiN/Carbon Coatings by Ion Beam Assistant Magnetron Spurting Deposition
J. Du and W.J. He 146

Adhesion Studies of Diamond-Like Carbon Films on 202 Stainless Steel Substrate with a Silicon Interlayer
L. Ji, H.X. Li, F. Zhao, J.M. Chen and H.D. Zhou 151

Study on Interfacial Bonding Strength of TiN Films Prepared by Magnetron Sputtering at Low Temperature
X.Q. Bai and J. Li 155

Rf Sputtering of Composite Fluorocarbon/ZnO Films and their Basic Properties
Y.H. Zhang, Q. Ji and X. Wang 159

Effect of Yttrium(Y) Content in Al Target on the Thickness of CrAlTiN Film by Magnetron Sputtering
Z.Z. Liu, Y.H. Liu, B.L. Jiang and S.R. Yu 163

Effects of Substrate Bias Voltage on the Microstructure of Cr-Al-N Coatings
M. Zhu, S.W. Duo, T.P. Li, M.S. Li and Y.C. Zhou 167

Effect of Low-Energy Ion Irradiation on Synthesis of Hard and Superhard Films
Z.G. Li, S. Miyake and Y.X. Wu 172

The Microstructure and Properties of CrN_x Films Synthesized by Unbalanced Magnetron Sputtering
Y.P. Wu, Y.X. Leng, S. Hong, S.F. Zhu, N. Huang, B. Bai and P.C. Zhang 176

Microstructure and Properties of TiC Coating by Vibrating Electrospark Deposition
C. Luo, S.J. Dong and X. Xiong 180

Effects of Incident Angle on Microstructure of Ni-Cr Film Deposited by PVD
Y.C. Shan, J.J. Xu, X.D. He and M.W. Li 184

Microstructure and Hardness of Ti-Si-C-N Coatings
Y. Guo, S.L. Ma, K.W. Xu, T. Bell, X.Y. Li and H.S. Dong 188

Influence of Bi-Layer Thickness on the Structure and Properties of Multilayered TiN/CrN Coatings by Cathodic Arc Plasma Deposition
C.L. Chang, W.Y. Ho, W.J. Liu, J.J. Hwang and D.Y. Wang 192

. Electrodeposition and Electroless Deposition

Microstructure and Properties of Surface Coating for Cr12MoV Steel Treated by TD Salt-Bath Vanadizing Process
M.B. Yang, L.W. Tang, H. Yang and W.L. Zhao 196

Study of Hard Chromium Plating from Trivalent Chromium Electrolyte
B.S. Li and A. Lin 200

Microstructure and Formation Mechanism of Aluminized Coatings on Nickel-Based Superalloys
J.B. Pei, L.W. Zhang, J. Niu and Q.Z. Zhang 204

Effect of UV-Irradiation on Anodized Films Formed on Titanium in 0.1M H_2SO_4 Solution
Y.H. Yao, H. Nanjo, J.N. Liu, Z.B. Xia, Z.P. Wang and J.F. Wei 208

Preparation and Property of Electrodeposited Zn-Fe-SiO_2 Composite Coating
Y.Y. Fan, Y.J. Zhang and P. Dong 212

Effect of pH Value on the Electrodeposition Potential of Cu-In Alloy Film
H.X. Yang, Z.L. Song, Y.W. Song and H. Zhang 216

On the Properties of Conductive Adhesive Filled with Electroless Silver Plated Flake Graphite
M. You, L.L. Zhang, Z.P. Gong, W.J. Liu and A.P. He 220

Preparing an Environment-Benignly Rare-Earth Based Chemical Conversion Coatings on 6063 Aluminium Alloy
D.C. Chen, G.X. Wu, W.F. Li, W.H. Gong and Y.Q. Liang 224

Cerium-Phytic Acid Passivation Treatment on Galvanized Steel
G.M. Liu, L. Yang, F. Yu, J.H. Tian, S.W. Duo and N. Du 228

Electrodeposited Ni/Al_2O_3 Composite Coating on NdFeB Permanent Magnets
H. Zhang, Y.W. Song and Z.L. Song 232

The Study of the Electrochemical Graining Process in $NaBO_2$- H_3BO_3 Solution and Grain Appearance on the Surface of Aluminum Alloy
J.Q. Liu, X.H. Wang and J.L. Xu 236

Study on Electroless Ni-P Deposit on W-Cu Alloy and its Anti-Corrosion Mechanism
L. Hao, Y.M. Zhang, C. Yang, H. Zhu, X.H. Mao, A. Lin and F.X. Gan 240

Sediment Co-Deposition of Nanostructured Ni-Al_2O_3 Composite Coatings
Q.Y. Feng, T.J. Li, H.Y. Yue, F.D. Bai, K. Qi and J.Z. Jin 244

The Effect of Substrates on Properties of Anodic Coatings Formed on Mg and Mg Alloys
R.F. Zhang, D.Y. Shan and E.H. Han 248

Anodic Alumina Oxide Template with Branched Structure Formed in Phosphoric Acid
H. Wang, H.W. Wang and P. Zeng 252

Study of Corrosion Performance of Electroless Ni-P Coating with Molybdenum Disulfide Nanoparticles
X.G. Hu, W.J. Cai, J.C. Wan, Y.F. Xu and X.J. Sun 256

Research of Microstructure and Properties of the 4Cr14Ni14W2Mo Steel with QPQ Salt-Bath Nitriding
G.Y. Xiong, B.L. He and R. Zou 260

Deposition of Amorphous Diamond Films on Different Substrates by Electrolysis of Methanol Solution
Y.Y. He, G.F. Zhang, G.Q. Li and X.D. Hou 264

The Study on the Deposition Efficiency of Microarc Oxidation on Aluminum Alloy
Z.J. Yan, X.H. Zhu, D. Cheng, Y.Z. Gao and L. Yan 268

Electrodeposition of Aluminum on 316L Stainless Steel from Molten Salts Based on Chlorides
Y.J. Wang, X.X. Ma and G.W. Guo 273

Preparation and Characterization of Cr-Co-P Alloy Coating Electrodeposited from Trivalent Chromium Solution
Y.M. Zhang, D.J. Fang, L. Hao, A. Lin and F.X. Gan 277

The Study on the Dispersants and Structures of Ni-P-α-Al_2O_3 Composite Electroless Plating Coating
L.M. Feng, K.G. Liu and X.F. Guo 281

Microstructure and Properties of Brush Electroplated Nano-SiC-Al_2O_3/Ni Composite Coating
H. Yang, S.Y. Dong and B.S. Xu 285

. Energetic Beams and Plasma Surface Treatments

Current Status of Supersaturated Surface Engineered S-Phase Materials
T. Bell 289

Low-Temperature Plasma Surface Modification of Medical Grade Austenitic Stainless Steel to Combat Wear and Corrosion
J.P. Buhagiar and H.S. Dong 296

Microstructural Features of EB-PVD Thermal Barrier Coatings Irradiated by High-Intensity Pulsed Ion Beam
C. Liu, X.G. Han, X.P. Zhu and M.K. Lei 300

Fabrication of SiC Particulates Reinforced $MoSi_2$ Composite Coating by Laser Cladding
S. Yang, M.R. Wang, T. Gong and W.J. Liu 304

Thermal Stability of Nitrogen Expanded Austenite Formed by Plasma Nitriding on AISI304 Austenitic Stainless Steels
L. Wang, Y. Li and Y.Z. Wang 308

Controlled Plasma Nitriding for an Optimum Balance between PACVD TiBN Coating Scratch Resistance and Substrate Toughness
Y. He, I. Apachitei, J. Zhou, T. Walstock and J. Duszczyk 312

Stacking Faults in a High Nitrogen Face-Centered-Cubic Phase Formed on Nitrogen-Modified Austenitic Stainless Steel
J. Liang and M.K. Lei 318

The Finite Element Simulation Research on Stress-Strain Field of Laser Cladding
P. Zhang, L. Ma, J.P. Yuan, X.N. Yin and Z.H. Cai 322

Electron Beam Surface Alloying of a Magnesium Alloy with Al
H. Ye and Z.L. Yan 326

Technical Study of Exhaust Valve Overlaying Based on Micro-Plasma Arc Welding
Y.H. Xiang, B.S. Xu, Y.H. Lv and D. Xia 330

Visual Study on Surface Micro-Topography and Residual Stress of Sheet Metal after Pulsed Laser Peening
S. Huang, J.Z. Zhou, J.J. Du, Y.Q. Sun and M.X. Ni 334

Microstructure and Tribological Properties of Layer Deposited by Micro-Plasma Arc Welding on Worn Gear
C.L. Liu, Y.H. Lv, B.S. Xu and D. Xia 338

Study on Process of Ion Implantation on AZ31 Magnesium Alloy
H. Zhou, F. Chen, Y.G. Yang, H.C. Wan and S. Cai 342

Preparation of Ag Nanoparticles Colloid by Pulsed Laser Ablation in Distilled Water
B. Xu, R.G. Song, P.H. Tang, J. Wang, G.Z. Chai, Y.Z. Zhang and Z.Z. Ye 346

Change of Hydrophobicity on Silicone Rubber Modified by CF_4 Capacitively Coupled Plasma and Inductively Coupled Plasma
S.H. Gao, Y. Liu, M.K. Lei and L.S. Wen 350

Experiments of Laser Surface Engineering for the Green Remanufacturing of Railway Coupler
C.Y. Liu, L.Y. Yu, W. Tian and J.C. Tang 354

Ultrasonic Characterization of EB-PVD Thermal Barrier Coatings Irradiated by HIPIB
L. Lin, Y. Zhao, J. Chen, X.M. Li and M.K. Lei 358

Numerical Simulation on Molten Process of GaAs Target Bombarded by Intense Pulsed Ion Beam
J.J. Sun, J.F. Li, Z.D. Liu and G.Q. Li 363

Electrical Conducting Coating on Glass Substrate Deposited by Wire Exploding Spray Coating Method
J.Z. Yang, Z.Y. Liu, D.W. Xu and T.J. Liu 367

Surface Modification of CrN Coating by Plasma Oxidation Process
W.Y. Ho, H.C. Chen, C.L. Chang, D.Y. Wang and W.Y. Ho 371

Microstructure and Wear Response of Ni/SiC Laser Cladding Composite Coatings on a Carbon Steel
B.Y. Lou, B. Xu, Y.B. Zhou, W.J. Bai and H.L. Du 375

The Structure and Corrosion Properties of Oxidized Layer Formed on Aluminium Alloy by Plasma Oxidation
Y. Li and L. Wang 379

A Numerical Simulation Studying for Plasma Expansion in Laser Ablation Processing
X.Y. Tan, Z.L. Wang, M. Feng and Y. Zhou 382

The Application of Ultrasonic Phase Spectrum of the Reflection Coefficient on Nondestructive Characterizing the Plasma Sprayed Coatings Irradiated by HIPIB
Y. Zhao, L. Lin, X.M. Li and M.K. Lei 386

Study on Wear Resistance of Plasma Sprayed Coating Remelted by Laser
Y.J. Liu, Y.S. Wang and X.C. Yang 392

Investigation of Mechanical Properties and Microstructure of Boron Films Implanted by Polyenergetic Nitrogen Ion
Z.H. Cai, P. Zhang, J.W. He, J.J. Zhao and J. Tan 396

The Remanufacturing System Based on Robot MAG Surfacing
S. Zhu, F.J. Meng and D.M. Ba 400

Investigation of Laser Shock Peening on Aero-Engine Compressor Rotor Blade
Z. Ma, Y.H. Li and C. Wang 404

Model of Heat and Mass Transfer in Atmospheric Pressure Plasma Arc (APPA) Cleaning Metal Surface
W.J. Xu, J.B. Meng, J.C. Fang and X.Y. Wang 408

Preparation and Characterization of Nickel-Based Composites Coatings Reinforced by TiB_2+WC on Stainless Steel by Laser Cladding
J. Li, W.G. Li and G.J. Zhang 412

Effect of Laser Scanning and Aging Treatment on Microstructure and Property of Austenitic Heat-Resistant Steel
B. Han, Y. Wang, Y.S. Li and R. Liu 416

Argon-Oxygen Post-Discharge Treatment of Hexatriacontane: Heat Transfer between Gas Phase and Sample
M. Mafra, T. Belmonte, A.M. Maliska, A.S. da Silva Sobrinho, U. Cvelbar and F. Poncin-Epaillard 421

Multiple Needle Cathodes Plasma Surface Alloying of Ti6Al4V with W-Mo-C-N
Y.F. Zhang, X.C. Bian, Q. Chen, G.Q. Zhang and Y. Gao 426

Influence of Oxygen Plasma Treatment on Surface Properties of Armos Fiber
P. Chen, J. Wang, C.S. Zhang, C. Lu, Z.F. Ding, S. Pan, W. Qi, J.C. Sun and J.F. Li 430

. Wear and Corrosion Behaviors of Engineering Surfaces

Preparation of Epoxy Modified Organosilicone High-Temperature Resistance Coatings
H. Zhu, Z.L. Chen, F. Nan, A. Lin and F.X. Gan 434

Research on Friction and Wear Performance of Brake Disc Pair Materials for New Type of Drilling Rig
X.H. Wang, S.W. Zhang and D.G. Wang 438

Influence of the Plating Conditions on the Structure and Corrosion Resistance of the Ni-Mn Alloy
S.L. Wang and W.W. Yu 442

Microstructural Evaluation of High Oxidation Resistant CrAlSiN Hard Coating at Elevated Temperature in Air Atmosphere
S.K. Tien, C.H. Lin, Y.Z. Tsai and J.G. Duh 446

Study on the Characteristics of Wear Resistance Using Silicate Particles as Additive on the Metal Friction Pairs
Y. Zhao, B.S. Xu, Y. Xu, P.J. Shi, X.L. Wang and B. Zhang 452

Effect of Microbes on the Early Corrosion Behavior of Carbon Steel in Eutrophic Lake
L.W. Jiang, G. Cao, X.H. Mao and F.X. Gan 456

Corrosion Behavior of AZ31 Magnesium Alloy with Microarc Oxidation Film Irradiated by High-Intensity Pulsed Ion Beam
X.G. Han, P. Li, X.P. Zhu and M.K. Lei 460

Design and Development of Sulphidation Resistant Coatings
H.L. Du, P.K. Datta and B.Y. Lou 464

Microstructure and Wear Behavior of Arc Sprayed WC-Co /FeCrB and WC-Ni /FeCrB Composite Coatings
B.Y. Fu, D.Y. He, J.M. Jiang and X.Y. Li 468

Preparation and Characterization of γ-Aminopropyltrimethoxysilane and Octadecyltrichlorosilane Self-Assembled Monolayers on Titanium Films
C.G. Sun and H.C. Zhang 472

Study on Friction Reduction and Anti-Scuffing Technology of Duplex Ion Nitrocarburizing and Sulphurizing
C.H. Hu, S.N. Ma, Y.L. Qiao, J.P. Zou, Y.D. Gao and X.F. Sun 476

The Growth Behaviors of IMC Layers at Soldered and Diffusion Bonding Sn/Cu Interfaces and the Effects of High Magnetic Field
C.Q. Cheng, J. Zhao, Y. Xu and P. Yang 480

Real-Time Measurement of Friction Coefficient in the Frictional Performance Test of Brake Disk
X.J. Huo, R.Q. Zhang, H. Wang, D.P. Qian and J.X. Teng 484

Tribological Behavior of Nano-Silicate Mineral Powder as Lubrication Oil Additive
B. Zhang, B.S. Xu, Y. Xu, X.L. Wang and Y. Zhao 488

Experimental Study for Cutting Performance of $Ti_{(1-x)}Al_xN$ Coated Drills
X. Yang, H. Kumehara and W. Zhang 493

Micro-Raman Analysis on Scratch of Si Surface Modified by Ion Implantation
Z.K. Lei, X.M. Pan, G. Liu, H. Yun and Z.X. Mu 497

Cavitation Behavior of Cast Iron under Different Parameter Conditions
Y.Z. Gao, T.N. Wang, Z.W. Yu and H.C. Zhang 501

Structure and Properties Investigation about a Copper-Base SHS Welding Material
J.Z. Hu, S.N. Ma and X.R. Chen 505

The Study of the Boundary Lubrication Mechanism of BN-C-Silicone Oil Composite Colloid at High Temperature
H. Guo and Z.M. Liu 509

Two Surface Treatment Processes and Their Influence on Magnesium Electrochemical Activity
J.Q. Liu, R.F. Zhao and N.B. Li 513

Contributions of Surface Engineering to Military Equipment Maintenance
L. Li and L. Chen 517

Structure and Wear Resistance at Elevated Temperature of Auto Brush-Plating n-Al_2O_3/Ni Composite Coatings
B. Zhang, B.S. Xu, S.Y. Dong and B. Wu 523

Wear Behaviors of Laser Cladded Nickel-Based Alloy Coatings Reinforced by Molybdenum and Cerium Dioxide under Sliding Friction
J.P. Yuan, P. Zhang, Z.J. Liang and L. Sun 527

Study on Anti-Corrosion Epoxy Resin Coating without Solvent
Q. Huang, Z.J. Liang and F.K. Xie 531

Research on Wear Mechanism of Surface Build-Up Welding Material of Brake Disc for Drilling Rig
X.H. Wang, S.W. Zhang and D.G. Wang 535

Mathematical Model of the Part Surface Temperature Field
J.H. Du, G.M. Liu and W.Z. Han 539

Interfacial Reactions in Sn-xZn-Cu/Cu Couples during Soldering
N. Zhao, J.H. Wang, H.T. Ma and L. Wang 543

An Impact-Abrasion Resistant Surfacing Electrode and its Wear-Resistant Mechanism
Z.J. Liu and X.B. Zeng 547

Application of Surface Engineering Techniques to Corrosion Control over Offshore Engineering Equipment
X.Q. Pan and J.J. Wang 551

Application of EIS and SEM to Study the Corrosion Behaviors of Organic Coatings/Substrate System
R. Yan, H. Wu, S.K. Yu, S.N. Ma and B.S. Xu 556

Effects of Shape and Distribution of M_7C_3 on Wear Resistance of Iron Based Composite
Z.J. Liu, Y.H. Su and J.G. Sun 560

Friction and Wear Behavior of Plasma Sprayed Nanostructured and Conventional WC-Co Coatings under Water Environment
X.Q. Zhao, J.M. Chen and H.D. Zhou 564

High Temperature Tribological Behavior of Nano-Al_2O_3 in Different Base Oils
X.F. Sun, Y.L. Qiao, J.W. He, S.N. Ma and C.H. Hu 568

Formation Mechanism of the Frictionally-Formed Protective Coating by Using Self-Repairing Material under Sliding Friction
W.G. Chen, Y.Z. Gao, H.C. Zhang and Y.J. He 572

Contact Failure Analysis of Nitrided 32Cr2MoV Coated with TiN by Multi-Arc Ion Plating
H. Li, H.B. Xu and J. Zhang 576

Preparation and Tribological Properties of Surface-Coated Nano-Copper Additives
Y. Xu, H.L. Yu, B.S. Xu, X.L. Wang and Q. Liu 580

Effects of Erosion Rate on the Erosion-Corrosion Synergism of High Velocity Oxy-Fuel Sprayed Ni-Based Coatings
A.F. Zhang, Y.Y. Wang and C.J. Li 585

Research on High-Temperature Corrosion-Resistance Performance of Exhaust Pipe of Heavy Duty Vehicle
S.C. Wei, B.S. Xu, H.D. Wang and G. Jin 589

Effect of Plasma Sprayed Coatings on Stress Corrosion Cracking of 08Cr2AlMo Steel in Saturated H_2S Solution
Y.F. Zhang, B.Q. Gu and Y. Ding 593

Wear and Corrosion Resistance of Ni-PTFE-SiO_2 Composite Coating Deposited by Jet Electrodeposition
W.S. Lin, S.Q. Qian and X.W. Chen 597

Lead-Free Oxidation- Resistant Glass-Ceramic Coating for Heat Processing of Ti-6Al-4V Alloy
M.W. Zhang, C. Gao, Y.X. Ding, J. Tao and T. Wang 601

Erosion Wastage at High Temperature for Arc Spraying Coatings
J.Z. Hu, S.N. Ma and X.R. Chen 605

. Functional Films and Coatings

Corrosion Behavior of TiO_2 Coating on Magnesium Alloy AM60 in Hank's Solution
R.C. Zeng, W. Dietzel, J. Chen, W.J. Huang and J. Wang 609

Deposition of Bioactive Titania Layers on Non-Metallic Substrates under Ambient Conditions due to Hydrolysis of Titanium Oxysulfate Solution
F. Xiao, R.G. Song and A. Osaka 613

Research on the Surface Treatment of Magnetic Powder in Bonded Nd8Fe80B6Co6 Alloy
H.F. Zhao, L. Wang and J.Y. Su 617

Enhanced Up-Conversion Emission of Er^{3+}-Doped Al_2O_3 Powders by Y^{3+} Codoping Prepared in a Non-Aqueous Sol-Gel Process
H. Wang and M.K. Lei 621

***In situ* Photoemission Study on Initial Growth of Er_2O_3 Films on Si(001)**
Y.Y. Zhu, Z.B. Fang, S. Chen, C. Liao and Z.M. Jiang 625

Surface Grafting Modification of Silk Fibroin by Atom Transfer Radical Polymerization
T.L. Xing, H.J. Wang, Z.X. Li and G.Q. Chen 629

Drug-Eluting Coronary Stents Coated with Polysulfone-Poly(ethylene Oxide) Block Copolymer by Ultrasonic Spray
X.Z. Gu, H. Yi, Z.H. Ni and J.H. Fang 633

Research on the Surface Treatment of Carbon Fibers Used in Fabrication of MMCs Wire
L. Wang and H.F. Zhao 637

Influence of the Surface Roughness of Plasma-Sprayed YSZ on LSM Cathode Polarization in Solid Oxide Fuel Cells
M. Gao, C.X. Li, M.D. Wang, H.L. Wang and C.J. Li 641

Preparation and Characterization of Poly Amide Amine (Generation 4.0) Self-Assembled Monolayer on Si (100)
B.F. Cui, J.M. Chen, J.Y. Zhang and H.D. Zhou 645

Self-Assembled Monolayers of Schiff Base on the Surfaces of Oxidized Copper
D.G. Li, X.J. Yu, Y.H. Dong, L.P. Zhang and Z.D. Zhao 649

Fabrication, Surface Modification and Analysis of Biocompatibility of Biologic Chitosan Scaffold
K.D. Song, P.F. Wen, T.Q. Liu, L.L. Jiang and G.Y. Mei 654

A Novel Thermo-Sensitive Polymer Film and its Imaging Properties
T. Wu, W.M. Zhang, N. Yang and J.L. Pu 658

Study on Preparation and Properties of a Room Temperature Fast Curing Epoxy Resin Nano-Adhesive
S.N. Ma, N.S. Zhu, C.Q. Li and C.H. Hu 662

Preparation of TiC/ Fe Surface Composite by a Casting–SHS Process
B.S. Jin, Y.F. Jiao and G. Li 666

Surface Modification of Nano-Copper and its Dispersive Behavior in Water
X.J. Wang, D.S. Zhu, X.F. Li and N. Wang 670

Preparation and Characterization of Cu-Coated Nano SiC Composite Particles
S. Zhu, C. Li, J.H. Du and W.Z. Han 674

The Synthesis and Phase Behavior of a Novel Discoticnematic Triphenylene Mesogen and its Application to an Optically Anisotropic Film
C.X. Zhang, Z.Q. He, J.L. Pu, J.J. Wang, Y.S. Wang, Z.X. Li and S. Ye 678

The Insulated Effect of New Inorganic Coatings on the Surface of Fiber Paper
F. He, X.D. He, J.F. Li, M.W. Li and S.M. Zhang 682

A Photometric Method for Measuring Photoacid Generator Efficiencies Using Rhodamine B as Acid Sensor in Thin Polymer Films
J.P. Li, W.M. Zhang and J.L. Pu 686

Superficial Optimization of Microcapsule
S.N. Qiao, L.H. Li, W. Ming and L.X. Mo 690

Controlled Self-Assembling Patterns of Colloidal Crystal by Solvent Modification
J. Wang, Y.C. Hu, B. Qu, B.P. Wang and Z.Z. Gu 694

Preparation and Characterization of Silver Citrate Nano-Emulsion and Nano-Silver Film
L.X. Mo, L.H. Li, Y.L. Li, Z.X. Li and M. Wang 698

Surface Modification and Properties of SiO_2 Nano Porous Aerogels
X.Y. Ni, Y. Li, Z.H. Zhang, J. Shen, B. Zhou and G.M. Wu 702

Encapsulated Titanium Oxide with Al_2O_3 and its Ultraviolet Shielding Properties
J.H. Li, X.W. Wu and J. Yang 706

Microstructure and Thermal Behavior of Gradient Bioceramic Coatings Fabricated by Laser Cladding on Titanium Alloy
M. Zheng, D. Fan, X.K. Li, Q.B. Liu and J.B. Zhang 710

Evaluation and Analysis for the Surface Morphology and Mechanism Properties of the Self-Repair Microcapsule
Y. Xin, W. Zhang, S. Zhang and B.S. Xu 714

The Effects of Surface Modifications on Tin-Doped Indium Oxide Films: Optoelectrical, Wettability and XPS Investigations
Z.Y. Zhong and F.L. Sun 718

Bio-Derived Bone Surface Modification with Biomimetic Thin Film Coatings to Improve Mesenchymal Stem Cells Adhesion and Spreading
K.D. Song, P.F. Wen and T.Q. Liu 722

Study on the Structure and Electrochromism of WO_3 and Ti-Doped WO_3 Films
L.G. Wang, G.Q. Li, Y.R. Hu, W. Gou and M. Shi 726

Study on Electrical Properties and 1064nm Pulse Laser Damage of Vanadium Oxide Thin Film
X.R. Chen, J.Z. Hu, W.Z. Han and B.S. Xu 730

Influence of Hydrothermal Treatment in Deionized Water on Surface Morphology and Structure of Titanium with Biomedical Application by Microarc Oxidation
W. Li, L.Z. Chen and P.S. Pang 734

Preparation of Sn-Coated Mesophase Graphite Powders by Carbothermal Reduction
Y.R. Jhan, T. Fang, S.Y. Tsai and J.G. Duh 738

Room-Temperature Deposition of Nano-TiO_2 Coating by Vacuum Cold Spraying Using $TiCl_4$-Aagglomerated Nano-TiO_2 Powder for Flexible Dye-Sensitized Solar Cell
S.Q. Fan, C.J. Li, G.J. Yang, J.C. Gao, L.Z. Zhang, C.X. Li and Y.Y. Wang 742

. Surface Machining and Mechanical Processing

Study on the Machining of Plasma-Sprayed Al_2O_3 Coatings by Ultrasonic Vibration Cutting
G.M. Liu, Y.L. Song, L.L. Ma and F. Wang 746

Appearance of Mechanical Zinc Coatings and Superficial Pore Sealing Treatment
J.C. Ding, Z.D. Zhao, J. Lu and Y.Q. Sun 750

Experimental Investigation on Intensity and Residual Stress in Superficial Layers Induced by Water Cavitation Peening with Aeration
D.Y. Ju and B. Han 754

Formation and Control of 40Cr Grind-Hardening
G.C. Wang, H.J. Pei, J.Y. Zhang, C.Y. Zhang and Q.F. Li 758

Fractal Characteristic and Wear Prediction of Surface Micro-Topography of Laser-Textured Roller
H.B. Liu, D.P. Wan and D.J. Hu 762

Effects of Dimple Geometric Parameters on the Performance of a Laser-Textured Mechanical Seal
X.D. Peng, S.E. Sheng, J.Y. Li, X.M. Pan and S.X. Bai 766

Research on the Robotic Free Abrasive Polishing System for the Rapid Spray Metal Tooling
G.C. Han, M. Sun, H.O. Zhang and G.L. Wang 770

The Surface Coating Robot for Space Solar Cell Array Assembly
Z. Fu, W.X. Yan and Y.Z. Zhao 774

The Characteristic Analysis of the Surface Wave of Film under Different Surface Tension
S.L. Wang, Z.R. Wu, Y.L. Cheng, M. Liu and D. Lu 778

Design of Surface Finish Using Compound Processes of Grinding and Electrochemical Finishing Following Turning
P.S. Pa 782

A FEM Study on Thermal Stress in Laminated Composite
Z. Li, M. You, X.L. Zheng, M.R. Zhao and J.L. Yan 786

Interacting of Screw Dislocation with Stiff Imperfect Interface
S.X. Ma, H. Fan and H. Hu 790

Design of Ultrasonic Ejecting Gun Used for Surface Nanocrystallization Based on CFD
X.M. Wang, S.N. Ma, C.Q. Li, J.W. He and X.Q. Feng 794

Study on CMP Slurry and Technique of Silicon Dioxide Dielectric for ULSI
B.M. Tan, J.Y. Yuan, X.H. Niu, H.L. Shi, Y.L. Liu and C.X. Cui 798

Applications of Nanoindentation Techniques in the Field of Surface Coatings
H.M. Wang, P.J. Shi, H.L. Yu, W. Zhang and B.S. Xu 802

Figuration Control of Deposit in Friction Surfacing
X.M. Liu, Z.D. Zou, Y.H. Zhang, S.Y. Qu and X.H. Wang 806

The Investigation of Surface Nanocrystallization of Structural Steel Induced by Supersonic Fine Particles Bombarding
D.M. Ba, S.N. Ma, F.J. Meng and C.Q. Li 811

The Development of Apparent Density Measuring Apparatus of Magnetic Lubricating Oil
X.H. Li, X.L. Zhang, Z.F. Liu and Y.Q. Li 815

Study on Chemical Mechanical Polishing Technology of Copper
S.L. Wang, Y.J. Yuan, Y.L. Liu and X.H. Niu 820

Study on the Polishing Characteristics of the Magnetic Abrasives Finishing to the Slender Pipe
Y. Chen, F. Yan and C.Q. Zhu 824

Effect of High Pressure Waterjet Peening on Surface Strengthening Properties of 7075-T651 Aluminum Alloy
G.Q. Chen, D. Zhang, J.H. Song, Y.S. Zeng, Z.Q. Li and W.L. Zhou 828

Numerical Simulation of Residual Stress Field Induced by Ultrasonic Shot Peening
G. Ma, X. Ling and Y.S. Zeng 832

Study on the Cleaning and Descaling Anticorrosion Technology of Water Cooling Engine without Disassembling
H. Jiang, X. Zhang, Y.G. Yu, Z.G. Yu and X.B. Lan 836

Key Engineering Materials 373-374 (2008) pp 1-10

doi:10.4028/www.scientific.net/KEM.373-374.1

The Remanufacturing Engineering and Automatic Surface Engineering Technology

Binshi Xu

National Key Laboratory for Remanufacturing, Academy of Armored Forces Engineering, Beijing 100072, China

xubinshi@vip.sina.com

Keywords: Remanufacturing engineering, Surface engineering, Automatic technology, Intelligentized technologies

Abstract. Entering into the 21st century, remanufacturing engineering has been developed rapidly in China, Especially from 2005, lots of remanufacturing laws and regulations have been released. Remanufacturing engineering is the industrialization of high technology maintenance to the waste productions, and the advanced period of the maintenance engineering and surface engineering. The basic character of surface engineering is synthesis, intercross, compounding, and optimization. Surface engineering takes the "surface" as core. Nano surface engineering is the integration and creation between the nano materials and traditional surface engineering. To adapt the demand of remanufacturing industrialization, five kinds of automatic and intelligentized technologies, namely automatic nano electro-brush plating technology, automatic high velocity arc spraying technology, semi-automatic micro plasma arc welding technology, automatic laser cladding technology, and intelligentized self-repair technology, have been independently innovated.

Rapid Development of RM Engineering in China

Entering into the 21st century, the momentous strategy, namely developing circular economy and constructing saving-oriented society, is made by Chinese government. As one of the important components, remanufacturing engineering has been developed rapidly. Especially from 2005, lots of remanufacturing laws and regulations have been released.

In May 2005, the "Strategic Consultant Study on Constructing the Saving-Oriented Society", which the sub-project "4R Engineering" including remanufacturing was listed, was started by CAE. The General Report pointed that the remanufacturing ratio to waste mechanical products will be up to 50% in 2010 and to 80% in 2020.

In June 2005, the No.21 and No.22 documents, released by China State Department, pointed out that the government will support greatly the remanufacturing to waste electromechanical products, and the "Green Remanufacturing Technology" was listed as one of the technologies, which will be highlighted to develop and popularize by the government.

In Nov 2005, the document "Notification on Organizing the First Time Circular Economy Demonstration", released by National Development & Reform Committee (NDRC), et al, publicized the 42 demonstration enterprise lists. Remanufacturing was listed as one of four highlight areas. The only engine remanufacturing enterprise, Jinan Fuqiang Power Co. Ltd, is one of the remanufacturing area demonstration enterprises.

In April 2006, vice premier Zeng Pei-yan commented in the Report on Development of Vehicle Components Remanufacturing and Relative Countermeasures: "Agreeing on the remanufacturing demonstration in the automobile components, exploring the experiments, developing technologies, meanwhile getting ready for revising the laws and regulations".

According to the direction from vice premier Zeng, the series actions about automobile components remanufacturing have been organized by NDRC. The Chinese Automobile Industry Society was designated to establish a special study group, which He Guangyuan, former minister of Mechanical Industry ministry, and academician Xu Binshi were advisers. By now, the automobile enterprises such as Yiqi, Erqi, Shangqi, pay more and more attention to the automobile components

remanufacturing.

In 2007, the first “Circular Economy Law” in China, instituted by State Department, has been submitted to the Legal System Office of State Department, and will be released in Oct, 2007. The law mentions definitely “Electromechanical Products Remanufacturing” and its policies.

Connotation of Remanufacturing Engineering

Remanufacturing engineering is a general designation of all techniques and engineering treatments to maintain and rebuild worn products, which taking the productive whole life period design and management as instruction, taking the great upgrade of the performance of waste productions as goal, taking the good quality, high efficiency, energy-saving, environment-protecting as rule, and taking the advanced techniques and industrializing process as measures [1].

Simply, remanufacturing engineering is the industrialization of high technology maintenance to the waste productions. The important character of remanufacturing engineering is that the quality of the remanufactured productions is as same as or superior to that of the new productions, and the cost is only a half of the new one, saving energy 60%, saving materials 70%, and decreasing the bad influence to environments. The remanufactured products are not the used ones but belong to the new products.

The whole expense of production, from preliminary study, design, manufacturing, using, maintenance, to abandoning, was regarded as whole life period expense. The first half life, which only possessed 20-30% expense, was paid great attention in the traditional notion. Whereas the after life possessed 70-80% expense was ignored.

Surface Engineering and Nano Surface Engineering

The advanced surface engineering and nano surface engineering technology is the key technology of remanufacturing engineering.

Surface engineering is a system engineering [2] to obtain desired surface properties through surface coating, surface modification or duplex surface treatments on a pretreated metallic or non-metallic surface to alter its morphology, chemical composition, microstructure and stress condition. The basic character of surface engineering is synthesis, intercross, compounding, and optimization. Surface engineering takes the “surface” as core. The major advantage of surface engineering is that the surface functional coating, being superior to the substrate materials, can be prepared on the components by a lot of surface methods, to endow the properties such as temperature-resistance, anti-corrosion, wear-resistance and anti-fatigue with the components. Comparing with the substrate materials, the coatings are thin, small in area, but hand on the main shoulders of components.

There are three developing stages in surface engineering, namely single surface engineering, composite surface engineering, and today’s nano surface engineering [3].

The single surface engineering technologies, such as thermal spraying, electro-deposition, are beyond the rigor environment. The combined surface technologies that integrate two or more kinds of surface engineering technologies enable to obtain “1+1>2” optimum strengthening effects on material surface. The composite technology has been the “accelerator” to improve the surface performance.

The third stage is today’s nano surface engineering. Nano surface engineering is a system engineering that combining the nano materials and nano technology with traditional surface engineering, through particular processing techniques or methods to alter farther morphologies, compositions, microstructures of surfaces and impart them new properties much more [4]. In 2000, Professor Xu binshi presented firstly the concept Nano Surface Engineering in Chinese Mechanical Engineering.

Professor T. Bell, the international founder of surface engineering, foreign nationality fellow of CAE, academician of Britain Royal Academy of Engineering, praised greatly nano surface engineering. He determined to cooperative study the nano surface engineering with Chinese

colleagues. The project named Nano Composite Coating and Composite Surface Engineering Used in Advanced Car Components has been rated as the Sino-Britain governmental collaborative project of science and technology in 2002.

Automatic Surface Engineering Technology

Lots of surface engineering technologies, aiming at the repair and remanufacturing of damage components, were developed in the recent years, such as Materials Preparation and Forming Integration High Velocity Arc Spraying Technology [5], Nano Electric Brush Plating Technology [6], Nano Selfrepairing Antifriction Additive Technology [7], Nano Thermal Spray Technology [8], Nano Solid Lubrication Technology [9], as well as Residual Life Evaluation Technology [10].

The remanufacturing course if a process and manufacture course with industrialization and batch. To adapt the demand of remanufacturing industrialization, the surface engineering technology must be from manual to automatic. Therefore in the period of Tenth-five and Eleventh-five years, some automatic and intelligentized surface engineering technologies have been developed by our lab, to improve more the performance of surface coatings and quality of remanufacturing.

Automatic Nano Particle Composite Brush Plating Technology. The nano particle composite brush plating technology is one of the advanced remanufacturing technology. With it, nano-particle composite brush plating coating which has excellent performance can be prepared. The service temperature of the coating enhances from 200°C to 400°C, and the contact fatigue performance improves from 105 cycles to 106 cycles. And it has been succeed to apply to remanufacturing of arming component. For example, the life of the imported engine compressor blade which was remanufactured with nano particle composite brush plating technology was over 300 hours bench test. But the manual brush plating technique has many disadvantages, such as low production efficiency and high working intensity. And it should be mentioned specially that the quality of remanufacturing components by manual brush plating technique is affected by the skill of operator easily. Accordingly automatic nano-particle composite brush plating technology has been developed by National Key Laboratory for Remanufacturing on base of manual brush plating technology.

The automatic nano particle composite brush plating technology (ANPCBP) is one of the surface engineering technologies which can prepare excellent performance nano-particle composite coating. It achieves the process of brush plating automatically on base of virtual instrument technology and automatic control technology. The automatic process of brush plating has been achieved by solving the key problems of feeding solution continuously, using solution circularly, monitoring processing parameter of brush plating (brush plating voltage, current density and temperature of solution) and procedure of brush plating (switching process and monitoring thickness of coating) real-timely. A model machine has been developed (Fig.1).

Fig.1 The model machine of ANPCBP

The n-Al_2O_3/Ni composite coating prepared by the automatic brush plating is relatively dense and uniform and has a smaller crystalline microstructure than that of the coating prepared by manual plating (Fig.2).

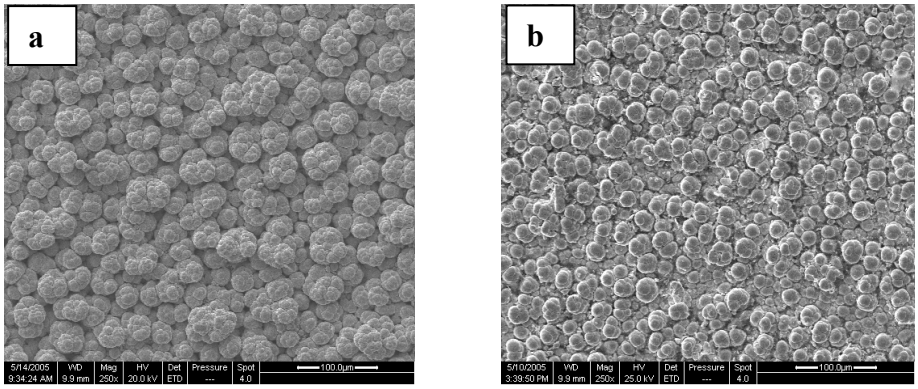

Fig.2 Surface morphology of n-Al_2O_3/Ni composite coating
(a) manual brush plating (b) automatic brush plating

Table 1 shows the micro-hardness of composite coating prepared by automatic brush plating and manual plating. It can be seen that micro-hardness of manual plating coating is uneven distribution and its hardness value shows great fluctuation in different micro-area. Micro-hardness distribution of automatic brush plating coating is more uniform than that of manual plating coating while hardness value of the former doesn't show great increment compared with the latter.

Coatings	Test load	Load time	Micro-hardness HV0.1				
	(g)	(s)	1	2	3	4	5
Auto	100	10	655	660	646	649	648
Manual	100	10	666	641	670	681	639

Table 1 Micro-hardness of nano-composite coating prepared by two methods

A special machine of automatic nano-particle composite brush plating, which is aimed at the batch remanufacturing problem of engine's connecting rods, has been developed on base of model machine and technology of automatic brush nano-particle composite plating, in Fig.3. The special machine solves many actual problems in the batch remanufacturing, such as positioning accuracy, remanufacturing quality, continuous working and adjustment of contact. It achieves the automatization in remanufacturing process. The special machine can remanufacture 4 to 6 engine's connecting rods one time and reduces the working time from 60min to 30min. This increases the production efficiency and reduces working intensity greatly. Consequently, it accelerates the development of demonstration plant for remanufacturing.

Automatic High Velocity Arc Spraying Technology. The high velocity arc spraying technology is a type of coating preparing process that using the ultrasonic air flow to atomize the melted metal wire feed stocks and drive the atomized jet to the surface of substrate, thus the flying particles deposit on the substrate from layer to layer. As compared with traditional are spraying technology, the high velocity arc spraying technology has such advantages as higher stability, higher processing efficiency and the coating has more compact structure. The new method of using the Fe-Al/ Cr_3C_2 cored wire to prepare inter-metallic compound and ceramic composite coating by high velocity arc spraying technique, has been independent innovated by NKLR, and is applied in boiler pipes of power station resistant from high temperature corrosion and erosion-corrosion, to realize the integrated processing of preparing Fe-Al inter-metallic compound and forming coating. The serving period of both Fe-Al/Cr_3C_2 coating and TAFA 45CT coating is about 3 to 5 years, but the maintenance cost per year of the former coating is only 50 percent of the later, which implies the Fe-Al/ Cr_3C_2 coating has a wide applying prospect in the field. The 1Cr18Ni9Ti/Al "pseudo" alloy coating is prepared by the on high velocity arc spraying technology has been successfully applied in remanufacturing STYER automobile engine block and crankcase. It has been established that, due to the micro-poles in the coating has the ability of oil-storing, the wear resistance of the pseudo alloy coating is about 9% higher than that of the traditional 1Cr18Ni9Ti coating under the oil lubrication sliding condition. The decrease of hardness of the pseudo alloy coating is easy for the

subsequent mechanic processing.

The newly developed automatic high velocity arc spraying technology combined the advantages of automatic technology based on industry robot and high-velocity technology based on new design of spraying gun, using the motion arm of robot or auto-operate machine to fix the high velocity arc spraying gun, planning the moving path of the gun based on the control software, adjusting the spraying parameters in real-time and controlling the gun worked under the pre-decided programs. The developed automatic spraying system contains four units, rectangular Cartesian coordinate auto-operate machine with four motion freedoms, high load-supporting positioner with two freedoms, center controlling unit and arc spraying equipments. The system has such features as, 1) the motion devices has six freedoms that enhanced the spraying stability; 2) the optimized controlling unit enables the wholly automatic action; 3) the real-time adjusting or controlling process increases the accuracy of spraying process; 4) the optimized configuration of spraying gun improves the quality of coating; 5) the development of inverse power supply improves the arc stability.

As compared with the manual arc spraying process, the automatic spraying process makes the thickness of deposited coating more uniform and improves the coating quality. On the other hand, the automatic spraying process let the workers far away from the high strength and polluted environment (high temperature, dense dust and strong noise), and increase the working efficiency. This automatic spraying technology is suitable for spraying several types of metal wires, such as cord wires, pseudo alloy wires and some special alloy composite wires. This technology has been accepted by the Jinan Fuqiang Power Co. Ltd to remanufacture the automobile engine block and crankcase and other typical parts, which enhances the performance, decreases the cost, saves the materials and energy, and improves the efficiency. Illustrationally, the remanufactured crankshafts use the discarded crankshaft as workblanks, thus it saves a great deal of rough stocks as compared with that of producing a new crankshaft. In addition, the remanufactured crankshafts avoid the nitridation process in the condition of 400°C high temperature for about 8 hours. It will take about 1.5 hours to remanufacture an engine crankcase by manual arc spraying process, but by automatic arc spraying technology it will decrease to 20 minutes. Fig.4 shows the arc spraying process of using the automatic high velocity arc spraying technology to remanufacture a discarded engine block, and the remanufactured domain (i.e., the crankshaft bearing shell hole) is shown in Fig.5.

Fig.4 Process which the AHVAS technology remanufactures a discarded STYER engine block

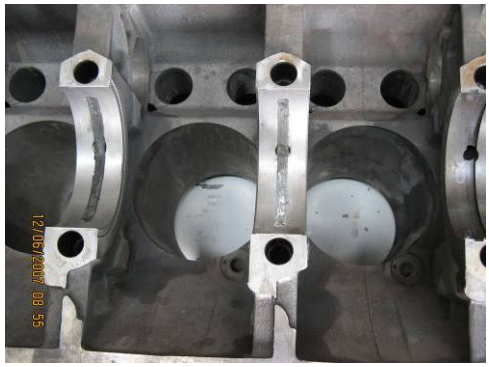

Fig.5 The remanufactured crankshaft bearing shell hole (after machining process)

Semi-Automatic Micro Plasma Arc Welding Technology. The micro plasma arc welding (MPAW) technology is the plasma welding technique with the current less than 30A. Semi-automatic MPAW utilizes micro-plasma arc to melt the metal power, clad another type of metals on the surface of remanufacturing or repairing components under the control of computer or single-chip computer. The micro-PAW system is developed by National Key Laboratory, which includes the micro-PAW power, the operation station, the positioner, powder-feeder system, and the gas-feeder system, as shown in Fig. 6.

The bonding between the cladded layer prepared by MPAW and substrate is metallurgical bonding, and it avoids the problem that the spray coating tends to flake away under the impact load

Fi.g 6 micro-PAW system

or alternate load. MPAW has a high current density and a low heat input, therefore, it can resolve effectively the problem which the components that are sensitive to the heat input can not be repaired by the other methods. And the deformation of the middle and small sized components caused by the heat input is resolved. High frequency inverter MPAW power with the invert frequency of 70kHz, which is higher than the usual invert frequency of 20kHz, is independently developed by National Key Lab for Remanufacturing. As a result, the volume of the equipment decreases, the responding characteristic of the system increases, and the technological process of MPAW is more stable.

The characteristic of the semi-automatic micro plasma arc welding technology is so excellent that makes the remanufactured components have good performance, high efficiency, low cost, and energy-saving, materials-saving, environment-protection. The technology has an extensive application foreground in the field of remanufacturing, such as camshafts, Al alloy cases, crankshafts, etc.

The MPAW Technology has been utilized to remanufacture the sealing cone of the used engine exhaust valves. The ST6 and Ni25 power were employed. The deformation of the remanufactured valves decreases, and their hardness renew to the standard. The micro-hardness is listed in Table 2. The remanufactured valve were showed in Fig. 7

Samples	Substrate			Transition area			Cladding layer			Top of layer	
1 (ST6)	330.48	340.57	367.68	492.57	471.04	479.20	450.89	537.83	525.75	517.92	671.58	643.89
Average		346.2			473.4				527.2			657.8
2 (Ni25)	330.48	340.57	367.68	403.44	407.19			412.09	448.39	427.92	546.12	535.38
Average		346.2			405.3				429.5			540.8

Table2 The vickers hardness of the sealing cone of valve (HRC)

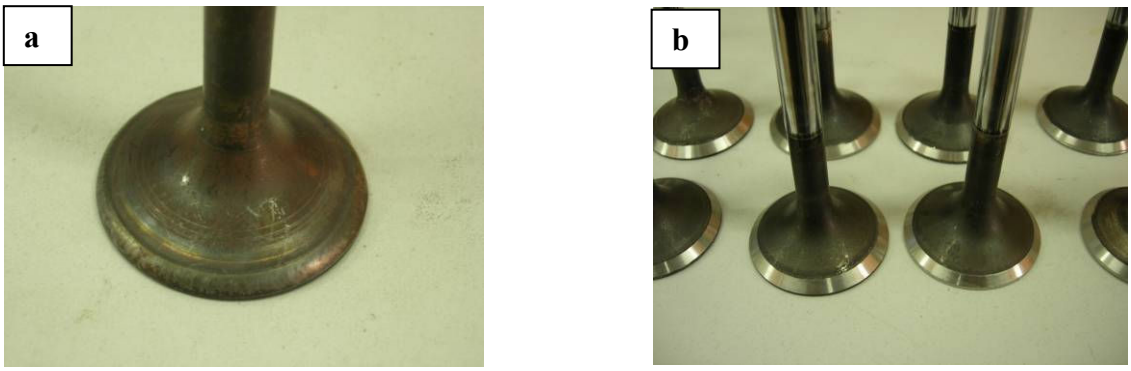

Fig.7 The remanufactured sealing cone of used engine exhaust valves
(a) Remanufactured and no machining (b) Remanufactured and machining and fit

Automatic Laser Cladding Technology. The laser cladding technology is the technology that the laser is used to heat the damage surface to melt the cladding materials and substrate, and then the metallurgic layers with lower dilution and excellent properties are rapidly formed. The performance of remanufactured components, such as wear-resistance, anti-corrosion, heat-resistance and oxidation-resistance is improved greatly.

The automatic laser cladding technology (ALCT) means a technology that the damage surface is repaired and remanufactured automatically by the laser operated by the industrial robot or operating-machine which has been input the moving programs and controlled by computer. This technology has many advantages, for instance, less distortion of substrate, metallurgic layers, superior properties, and less machining process after cladding.

ALCT has been successfully utilized to remanufacture the severe disabled tooth surface of heavy load gears by National Key Laboratory of Remanufacturing (seeing Fig.8). The problems, such as layer cracks, over heat in part of substrate, keeping the precision of gear surface and improving the properties, have all been resolved. The performance of wear-resistance and anti contact fatigue of the remanufactured components is up to the demand similar with new one.

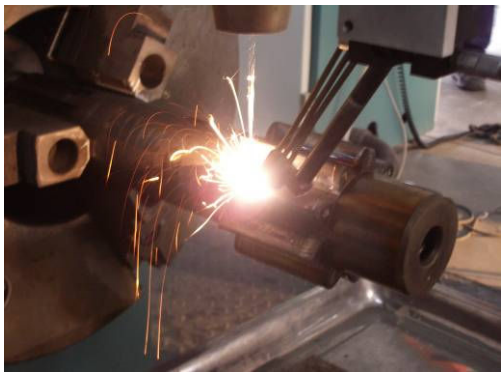

Fig.8 Automatic laser cladding remanufacturing to the tooth surface of heavy load gear

Due to its huge size, the CO2 laser that is used to laser cladding is not suit for the field operation. Meanwhile, the CO2 laser has the long wavelengths and low energy conversion rate. The absorption of cladding materials to laser energy is also lower. Therefore, the high-power fiber coupled solid laser and high power diode laser have been developed by our laboratory to realize the field rapid remanufacturing for the components, break through the technique limitation of laser cladding in field, and solve the key technique and theory problems, including new materials used for rapid formation remanufacturing, accuracy control and quality control to the remanufactured components formation (seeing Fig.9 and Fig.10).

Fig.9 Fiber coupled solid laser system with robot operating

Fig.10 The high power diode laser system with manipulator operating

Intelligentized Self-repairing Technology. The intelligentized self-repairing technology is a kind of technology that bases on the intelligentized biology technology and micro-nano technology, through the friction chemistry between the metal substrates and self-repairing materials, a reaction thin film with good friction reduction and self-repairing performance is formed on the worn surface, a dynamical equilibrium is achieved between wear and dynamic repair, and the self-repairing on the worn surface is realized without disassembly and shut down of the machine.

The Cu nanoparticles, with an average size of 20-50 nm, have been successfully prepared by liquid phase reducing method in National Key Laboratory for Remanufacturing. The high-energy mechanical decentralization method and surface modifying method were utilized to creatively solve the great problem that nanoparticles decentralize stably in the oil medium. Fig.11 and Fig.12 show the XRD spectra and TEM morphology of Cu nanoparticles, respectively.

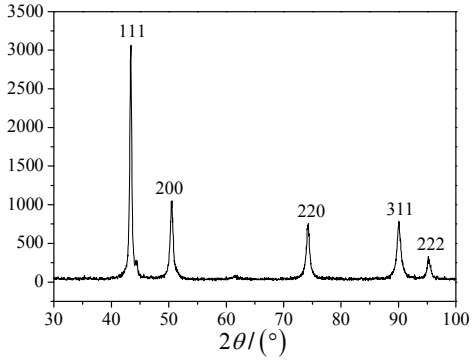

Fig.11 XRD analysis of Cu nanoparticles

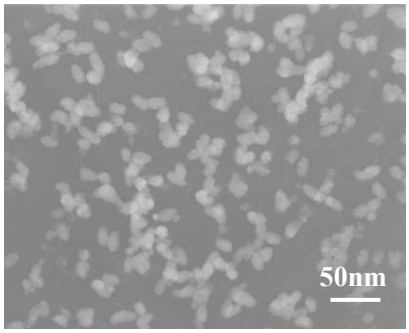

Fig.12 TEM morphology of Cu nanoparticles

A kind of the in-situ nano friction reduction and self-repair additive was independently prepared by our laboratory. Its formula is novel including the self-repairing elements such as Cu nanoparticles and rare earth compound, and other functional additives with the function of cleanness, dispersion, oxidation resistance and corrosion resistance. The additive is granted the national patent for invention in 2004.

The mechanism which the additive reduces friction, decrease wear and self-repairing was studied and explained. A protective Cu self-repairing film is formed on the worn surface after friction. The film possesses the excellent mechanical performance and friction reduction property, good bonding with substrate, and can in-situ repair the early damage on the worn surface and improve the lubrication.

The bench experiment for Jeep engine lasting 300 hours was carried out. The common oil was used in No.1 engine, and the oil containing the additive was used in No.2 engine. The endurance experiment results showed that the No.1 engine's maximum power and torque decreased, whereas

Total power		Maximal power/ rotating speed Kw/rpm	Maximal torque/ rotating speed Nm/rpm	Minimal oil consumption ratio/ rotating speed g/Kwh/rpm
No.1 engine	Before experiment	118.22/4500	280.04/2250	318.82/3000
	After experiment	114.72/4500	278.60/2250	317.26/3000
No.2 engine	Before experiment	112.52/4750	269.45/2250	310.97/2250
	After experiment	119.36/4750	274.82/2250	292.36/2250

Table3 Bench experiment results of Jeep engine with six cylinders

the maximum powder of No.2 engine increased by 6.08%, the maximum torque increased by 2% and the fuel consumption reduced by 5.98%, respectively. The above results indicate the good economical efficiency and power ability. Fig.13 shows the element analysis result of worn cylinder liner surface after 300 hours endurance experiment. It can be seen that a red protective film that composed of copper is formed on the worn cylinder liner surface. The film improves the lubricating condition of piston ring / cylinder frictional pairs and prolongs the service life of the engine.

The application test on the heavy-load vehicles with duration of 1.5 years was performed. The Results indicate that the lubricating conditions of the vehicles are improved obviously, wear of materials is reduced, dynamic performance is improved and machine oil consumption is reduced.

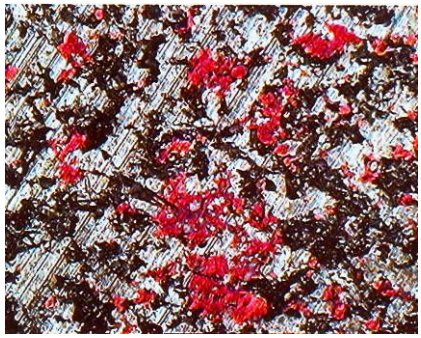

Fig.13 Element analysis result of worn cylinder liner surface

Conclusions

(1) Remanufacturing engineering is the industrialization of high technology repair and reformation to the waste productions. The important character of remanufacturing engineering is that the quality of the remanufactured productions is as same as or superior to that of the new productions, and the cost is only a half of the new one, saving energy 60%, saving materials 70%, and decreasing the bad influence to environments. The remanufactured products are not the used ones but belong to the new products.

(2) There are three developing stages in surface engineering, namely single surface engineering, composite surface engineering, and today's nano surface engineering. The advanced surface engineering and nano surface engineering technology is the key technology of remanufacturing engineering.

(3) Five kinds of automatic and technologies, namely automatic nano electro-brush plating

technology, automatic high velocity arc spraying technology, semi-automatic micro plasma arc welding technology, automatic laser cladding technology, and intelligentized self-repair technology, have been independently innovated. These technologies have been applied in the remanufacturing demonstration enterprise.

Acknowledgements

The paper was supported by NSFC (50735006), 973 Project (2007CB607601), 863 Project (2007AA04Z408), Consultative project of CAE (12/2002A) and Sino-Britain collaborative project (2002/209 M3).

References

[1] Xu B S.: Consultative report of China Academy of Engineering Vol. 12(2000), 12. (in Chinese)

[2] Xu B S.: *Theory and Technology of Surface Engineering* (National Defence Industry Press, China 1999)

[3] Bin-Shi Xu: *Nano Surface Engineering* (Chemical Industry Press, China 2004)

[4] Xu B S, Liu S C. *China Materials Engineering Canon*. (Chemistry Industry Press, China 2006)

[5] Xu B S, Zhu Z X and Zhang W.: Wear Vol. 257(2004), p.1089

[6] Xu B S, Wang H D and Dong S Y: Electrochemistry Communications Vol. 7(2005), p.572

[7] Xu B S, Wang H D and Liang X B: Proceedings of International Conference on Intelligent Maintenance Systems. 2003: 457-466.

[8] Zhu S, Xu B S.: Key Engineering Materials Vol. 280(2005), p.1203

[9] Xu B S, Liu S C and Liang X B.: Chinese Journal of Mechanical Engineering Vol. 39(2003), p.21. (in Chinese)

[10] Zhang X C, Xu B S. and Wang H D: Journal of Applied Physics Vol. 101(2007) p.083530~6

Key Engineering Materials 373-374 (2008) pp 11-14

doi:10.4028/www.scientific.net/KEM.373-374.11

Effect of Plasma Sprayed Ceramic and Cermet Coatings on Wear-out Failure of High Temperature Ball Valve

Lin LIU[1, a], Boqin GU [2,b] and Ye CHEN [3,c]

[1,2,3]College of Mechanical and Power Engineering, Nanjing University of Technology, Nanjing 210009, China

[a]liulin_02@sohu.com, [b]bqgu@njut.edu.cn, [c]njsb@saibotech.com

Keywords: high temperature ball valve, plasma sprayed coatings, wear-out failure, thermal shock property, bonding strength

Abstract. Three kinds of coating materials, namely Cr_2O_3 ceramic, Al_2O_3-TiO_2 ceramic and WC-Co cermet, were screened and sprayed on the surface of valve ball by plasma spraying technology, and two kinds of brush plating materials, namely high speed nickel and nickel tungsten, were also screened and brush plated on the surface of valve seat by electrical brush technology. The microstructure and morphology of the plasma sprayed coatings were analyzed by means of scanning electron microscopy. The tribological properties of the plasma sprayed coatings sliding against the high speed nickel and nickel tungsten layers were investigated on a pin-on-disc friction and wear tester. The microhardness, thermal shock property and bonding strength of the coatings were also tested. The results indicate that the sealing pair composed of the valve ball with the plasma sprayed coating of Al_2O_3-TiO_2 and the valve seat with the brush plating layer of nickel tungsten has the best combination property.

Introduction

The ball valves used in the reforming catalyst regeneration system in petrochemical plants operate usually under the conditions of elevated temperature, high pressure and mill dust. Gas-solid mixture with high hardness Al_2O_3 powder induces dry friction of the contact surface between valve ball and seat and causes excessive wear and scuffing of the sealing surface, which results in failure of ball valves finally. To increase wear resistance of the sealing surface is an effective means for elongating the lifespan of ball valves in order to improve the operating safety and stability of the reforming catalyst regeneration system.

Plasma spraying is often considered as a potential alternative to traditional coating manufacturing techniques (such as hard chrome electroplating) for the production of wear-resistant coatings [1–3]. Plasma sprayed ceramic and cermet coatings are technologically important materials as they find a lot of industrial applications [4].

In this paper, three kinds of ceramic and cermet coating materials, namely Cr_2O_3, Al_2O_3-TiO_2, and WC-Co, were screened and sprayed on the surface of valve ball by plasma spraying technology. The thermal shock property, bonding strength of the coatings, and the wear resistance of the sealing pairs composed of plasma sprayed coatings and brush plating layers were investigated, and the optimum sealing pair of the high temperature ball valve was obtained.

Experiment details

Table 1 Deposition condition and thickness of plasma sprayed ceramic and cermet coatings

Coating	Voltage [V]	Current [A]	Primary gas flow rate Ar [l min^{-1}]	Powder flow rate [g min^{-1}]	Carrier gas N_2 [l min^{-1}]	Spraying distance [mm]	Thickness [μm]
Cr_2O_3	30~50	320	36.7	30	17.7	95~100	100~150 50
Al_2O_3-TiO_2	30~50	360	36.7	28	13.3	95~100	50
WC-Co	30~50	360	36.7	30	13.3	95~100	50

Cr_2O_3, Al_2O_3-TiO_2 (Al_2O_3+13 wt% TiO_2), and WC-Co (WC+12 wt% Co) were deposited on the valve ball (martensitic stainless steel) by plasma spraying technology. The deposition conditions and thicknesses of the coatings are listed in table 1.

The microstructure and morphology of different plasma sprayed ceramic and cermet coatings were investigated by scanning electron microscopy (SEM). The coating microhardness was measured with a microhardness Vickers indenter according to ISO standard "Metallic and Related Coating-vickers and Knoop Microhardness" (ISO-4516-2002), and the mean values of 10 measurements were taken as the test results. The results obtained for a load of 200 g are given in Table 2.

Table 2 Mechanical properties of plasma sprayed ceramic and cermet coatings

	Hardness [Hv0.2]	Bond strength [MPa]	Thermal shock property [times]
Cr_2O_3	1429	39.35	64
Al_2O_3-TiO_2	1463	60.40	No visible failure
WC-Co	1285	45.97	8

Several tensile tests were carried out to measure the bond strength of the coating and the base material, according to ASTM standard "Standard Test Method for Adhesion or Cohesion Strength of Thermal Spray Coatings" (C-633-2001). The tests were conducted on an Instron universal material test system. The samples were tensioned with the speed of 0.015 mm/s till they were fractured. Calculated the degree of adhesion strength as Eq. 1 follows:

$$\text{Adhesion strength} = \text{maximum load}/\text{cross-sectional area}. \quad (1)$$

For each of the coating, five specimens were adopted, and the average value of five experimental data was taken as the bond strength.

In order to assess the thermal shock property, the samples were thermally cycled. Each cycle consisted of 15 min at 800°C, followed by water cooling to room temperature. The number of thermal cycles was 100 times or visible abscission or cracking was observed.

Tribological evaluation of coated substrates was performed using a pin on disc tribometer, according to ASTM standard "Standard Test Method for Wear Testing with a Pin-on-Disk Apparatus" (G-99-2004). Friction and wear properties were evaluated with the sliding nickel-base alloy (valve seat material) pins and the pins which were brush plated by high speed nickel or nickel tungsten with diameter of 5 mm and length of 12 mm against substrate specimen (martensitic stainless steel) and the coated specimens with diameter of 40 mm and length of 10 mm. The coated sample was affixed on the stationary shaft while the pin was mounted on the rotating shaft. All the coated specimens and pins were polished before tests. Surface roughness of the counter pairs were Ra = 1.25 μm. The normal load was set as 20 N, and the rotational speed of the pin was fixed as 190 rev./min (alinear sliding velocity of 460 mm/s). The total sliding length was set as 6621 cycles, which corresponds approximately to a sliding distance of 960 m. The variation of the friction coefficient was recorded as a function of the sliding distance. The volume loss of the coatings and pins was measured before and after tests to evaluate the wear performance of different sealing pairs.

Results and discussions

Microstructure of coatings. The typical SEM micrographs of the plasma sprayed coatings are shown in Fig. 1. In Al_2O_3-TiO_2 ceramic coating, the white layers are TiO_2 and the dark ones are Al_2O_3 (Fig. 1 C and D). The porosity of the coating is very low, due to more rounded pores produced by unmolten particles, splat stacking faults and gas entrapment. TiO_2 was well melted and partly mixed with alumina, as some highlight lamellar areas containing different amounts of titania can be seen from SEM micrographs. The intersplat adhesion of this coating is better than that of the other coatings. In Cr_2O_3 ceramic coating, there exit many micro pores (Fig. 1 A and B). In WC-Co coating, the micro pores are difficult to be found (Fig. 1 E and F). Of all the tested coatings, the microhardness of Al_2O_3-TiO_2 coating is the largest, while that of WC-Co is the smallest (table 2).

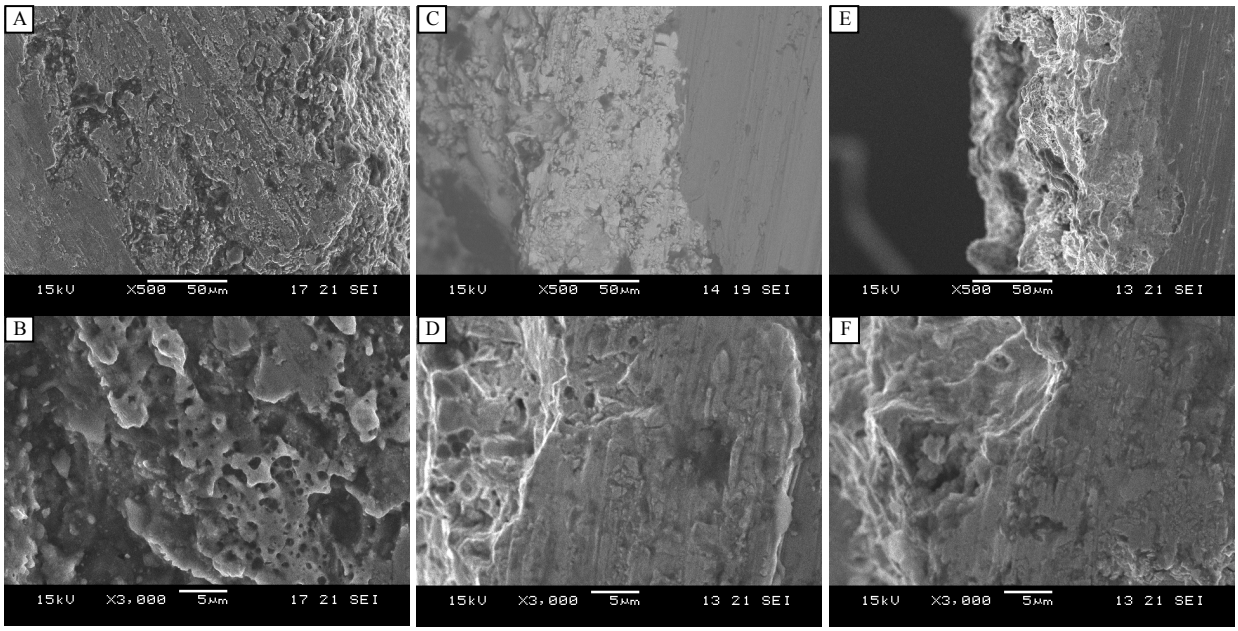

Fig. 1. SEM micrographs of coating cross-section.
A and B: Plasma sprayed Cr_2O_3 coating; C and D: plasma sprayed Al_2O_3-TiO_2 coating; E and F: plasma sprayed WC-Co coating.

Bond strength of coatings. The bond strength of the coating and the substrate has a significant effect on the service life of ball valves operating at high temperatures. The bond strengths obtained by tensile test are also listed in Table 2. The bond strength of Al_2O_3-TiO_2 coating and martensitic stainless steel substrate is the largest, and its average valve reaches to 60.40 MPa. The average bond strengths of Cr_2O_3 and WC-Co are 39.35 MPa and 45.97 MPa, respectively.

Thermal shock properties of coatings. It can be seen from table 2 that the three kinds of coatings deposited by plasma spraying have different thermal fatigue resistances. For the same thickness of coatings, Al_2O_3-TiO_2 coating has the maximum thermal cycles, and WC-Co coating has the minimum thermal cycles. It is well known that the thermal fatigue resistance of the coatings increased with the increase of relaxed thermal stress. Coatings having mismatched thermal expansion coefficient with the substrate, the interface of coatings create thermal stress when the specimens are heated. In the thermal fatigue resistance test, residual stress of the coatings presents cyclic variation following with coatings heating and cooling. Coating creates microcrack when the amplitude of the cyclic stress exceeds fatigue limit. Fragile WC-Co coating makes microcrack extension quickly until brittle fracture. Al_2O_3-TiO_2 consists of 13 wt% TiO_2. TiO_2 makes microcracks netlike disperse in Al_2O_3 coating, and these microcracks netlike result in the relaxation of thermal stress, which enhances thermal fatigue resistance of the coating effectively.

Tribological properties of coatings. Fig. 2 shows the variation of the friction coefficient with the sliding cycle for the different friction pairs. There exist two distinct steps during wear process: the "running-in" step and the stabilization step. In the "running-in" step, the friction coefficient increases obviously with sliding distance until it reaches to a certain value. Afterwards, the wear process is in the stabilization step, and the friction coefficient remains constant approximately until the test ends. For the martensitic stainless steel versus nickel-base alloy pin friction pair, the friction coefficient at the end of the "running-in" step is about 0.70, and it reaches to 0.80 in the stabilization step. For Cr_2O_3, Al_2O_3-TiO_2, and WC-Co coatings versus high speed nickel and nickel tungsten friction pairs, their friction coefficients at the end of the "running in" step are all lower than 0.40, and they remain at the nearly unchangeable values from 0.35 to 0.55 in the stabilization step.

Fig. 3 shows the wear rates of these friction pairs measured after a sliding distance of 960 m. The wear rate of the counter pins is larger than that of the plasma sprayed coatings, the wear rate of the substrate specimen versus nickel-base alloy pin friction pair is significantly larger than that of other friction pairs, and the wear rate of the WC-Co versus nickel tungsten friction pair is the least.

In the Cr_2O_3 coating worn, many pits and pores were observed. Pores and microcracks presenting in the coating act as crack initiation sites, leading to the coating spallation. Owing to the deformation

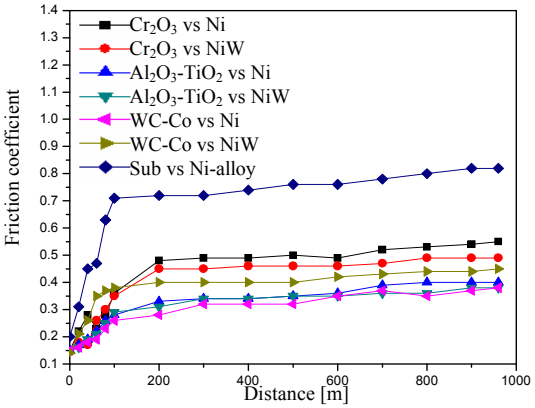

Fig. 2. Friction behaviors of different friction pairs.

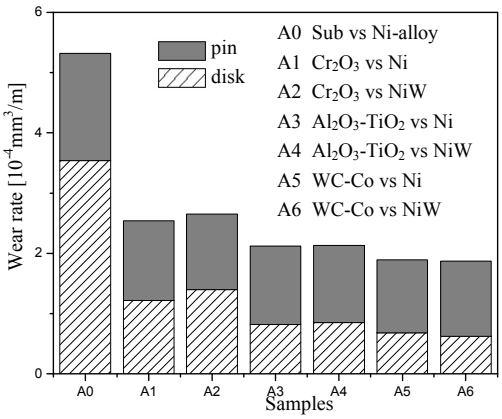

Fig. 3. Wear rate of disk-and-pin testing after sliding 960m

at the sliding interface, the Cr_2O_3 coating is crushed into wear particles, which result in the abrasive wear of the friction pair. Al_2O_3-TiO_2 and WC-Co coatings have lower porosity and fewer microcracks than Cr_2O_3 coating, and their wear rate is lower than Cr_2O_3.

Conclusions

(1) Plasma sprayed coatings have been widely used as protective layer of machine parts and pressure-containing components due to their good abrasion resistance, corrosion resistance and heat resistance. The friction behaviors of the martensitic stainless steel versus nickel-base alloy pin friction pair, and the Cr_2O_3, Al_2O_3-TiO_2, and WC-Co coatings versus high speed nickel and nickel tungsten friction pairs were investigated. The abrasion resistances of the friction pairs with sprayed coatings and brush plating layers are obviously better than that of the friction pairs without coatings or layers.

(2) TiO_2 is helpful for forming dense netlike microstructure in the Al_2O_3-TiO_2 coating, which prevents from the cracking propagation. Research results indicate that Al_2O_3-TiO_2 coating has the best bond strength and thermal shock property, the highest microhardness, and relatively small friction coefficient.

(3) In the seven kinds sealing pairs, the pair consisted of the valve ball with the plasma sprayed coating of Al_2O_3-TiO_2 and the valve seat with the brush plating layer of nickel tungsten has the best combination property. The valve with this kind of sealing pair has longer service life.

References

[1] H.J. Kim, C.H. Lee: Surface Coating Technology. Sci. Forum Vol. 139 (2001), p. 75

[2] S. Ahmaniemi, M. Vippola: Wear. Sci. Forum Vol. 252 (2002), p. 614

[3] T. Saharoui, N.E. Fenineche: Mater. Sci. Forum Vol. 152 (2004), p. 43

[4] R. Venkataraman, G. Das: Materials Science & Engineering. Sci. Forum Vol. A445 (2007), p. 269

Key Engineering Materials 373-374 (2008) pp 15-18

doi:10.4028/www.scientific.net/KEM.373-374.15

Preparation and characterization of Ni-Al-Cr_3C_2 coating

Ling-zhong DU[a], Wei-gang ZHANG[b], Deng-jun ZHANG[c] and Bao-hou LI[d]

Institute of Process Engineering, Chinese Academy of Science, Beijing 100080, China

[a]dulingzhong@hotmail.com Tel.: +86 10 62656037, Fax.: +86 10 62656037, [b]wgzhang@home.ipe.ac.cn, [c]djli@home.ipe.ac.cn, [d]bhli@home.ipe.ac.cn

Keywords: Flame Spray; Plasma Spray; Tribological properties.

Abstract. In order to improve the surface properties of the machine parts, the NiAl cladding Cr_3C_2 powder were flame and plasma sprayed. The morphology, microstructure, composition and wear properties of the coatings were examined. The results show that due to the exothermal reaction of the Ni and Al elements, the bonding strength of the coatings are improved, and the main compositions of the coatings are Ni_3Al inter-metallic compound and Cr_3C_2. The flame sprayed and plasma sprayed coatings show almost the same micro-hardness and friction coefficient. But the microstructure of the plasma sprayed coating is more compact than that of the frame sprayed one and the wear resistance of the flame and sprayed coatings is 30% and 120% higher than that of the 1045 steel, respectively. The main wear mechanisms of the coatings are plastic deformation and spallation, and the high bonding strength and the uniformly distributed Cr_3C_2 particles play important anti-wear roles.

1 Introduction

The presence of abrasive particles is an obvious source of accelerated wear to the fan in the steel works, which causes heavy economic losses. Thermal sprayed coatings are economical, can be produced by means of relatively simple techniques and offer excellent corrosion and wear protection. As a result, these coatings have found uses in various industrial applications [1,2,3]. In this paper, a new type of thermal spraying powder of NiAl/Cr_3C_2 was prepared and the tribological properties of the flame and plasma sprayed coatings were evaluated to verify the feasibility of the coating as a candidate wear protective material for the fan.

2 Experimental details

The differential scanning calorimetry (DSC) of the powders was conducted in a Netzsch STA449 thermal analyzer at a constant hearting rate of 20K/min from room temperature to 1000°C.

The sprayed coatings were deposited on 1045 steel substrates by APS-2000K plasma spray (China make) and HP-6K flame spray (China make) systems and the spray parameters were shown in Table 1. Before being coated, the substrate was blast cleaned with coarse Al_2O_3 particles and then applied the coating at a thickness of approximately 1.3 mm. After application, the sprayed coatings were ground to a thickness of 1.0 mm.

The micro-hardness indentations were made into the cross section of the coating to avoid the substrate effect.

The constituents of the coatings were characterized by X-ray diffraction (XRD) in a Philips X'Pert Pro diffractometer using filtered CuKα radiation (λ=0.1541nm).

The reciprocating friction and wear tests were carried out using an Optimal SRV "ball-on-disk" test equipment, consisting of a ball oscillating on a static disk (Φ24×7.88 mm^2). In these tests, the coated samples were used as static disks and the ball was ZrO_2 ceramic. All tests were commenced at a load of 70N, a time of 30min, a frequency of 30Hz, and a stroke of 1.5mm. The friction coefficient was recorded during each test, and the mean values were calculated. The wear volume was measured using Rank Taylor Hobson Talysurf 5P-120 system.

The surface morphologies of the powder and the coatings before and after wear testing were observed by SEM, as well as chemical qualitative and semiquantitative analysis by EDX.

Table 1 Thermal spray parameters

Flame spray	O_2 flow (m^3/h)	C_2H_2 flow (m^3/h)	Air flow (m^3/h)	Powder feed (g/min)
	1.0	0.8	2	50
	O_2 pressure (MPa)	C_2H_2 pressure (MPa)	Air pressure (Mpa)	Spray distance (mm)
	0.4	0.08	0.3	130

Plasma spray	Ar flow (L/min)	H_2 flow (L/min)	Carrier gas flow (m^3/h)	Voltage (V)	Powder feed (g/min)
	40	2.4	0.4	50	50
	Ar pressure (Mpa)	H_2 pressure (MPa)	Carrier gas pressure (MPa)	Current (A)	Spray distance (mm)
	0.65	0.45	0.3	600	100

3 Results and discussion

3.1 Characterization of the powders

Fig.1 shows that the NiAl/Cr_3C_2 powders have round morphologies, with a size of about 50~80 μm. The powders are prepared by two steps. First the nickel metal are precipitated onto the Cr_3C_2 core solid particles surface by reacting the dissolved salt with the hydrogen reducing gas at elevated temperature and pressure. And then the fine aluminium powders are bond onto the Cr_3C_2/Ni composites. The NiAl/Cr_3C_2 powders shows good sprayed properties with the flowability of 31s/50g and the apparent density of 2.4 g/cm^3. And the composite powders have a composition of 30Cr_3C_2-60Ni-10Al by weight. The DSC traces from the as-received powders in Fig.2 reveals that there is a broad exothermal peaks at the temperature of about 640°C. This exotherm is associated with formation of Ni-Al intermetallic compound [4,5,6,7] and is benefit to the improvement of the bond strength with the substrate.

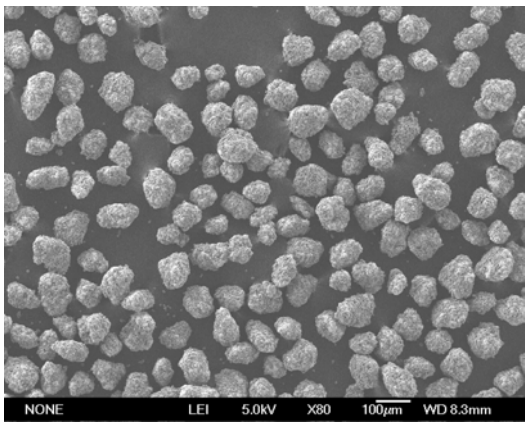

Fig.1 Morphologies of the NiAl-Cr_2C_3 powders

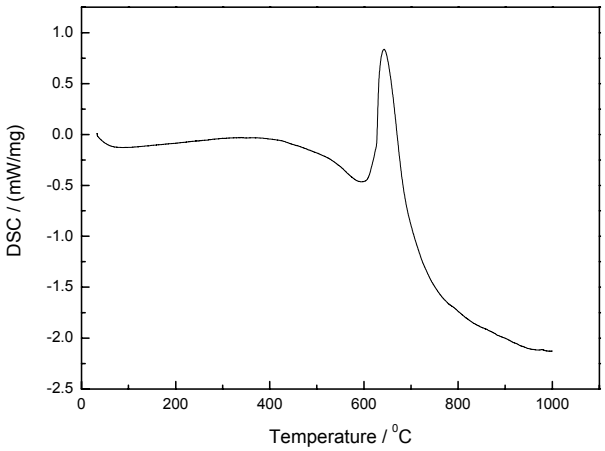

Fig.2 DSC trace from the NiAl-Cr_2C_3 powders

3.2 Microstructure and hardness

Fig.3 shows the cross-section morphologies of the flame and plasma sprayed coatings. It can be seen that both coatings presented a laminar microstructure, typical for the spraying process [8,9]. As expected, the microstructure of the plasma sprayed coating is more compact than that of the flame sprayed one. There are no pores and cracks at the interface, which shows that the interface bonding is firm. XRD analysis from the coatings surface in Fig.4 indicates the main constituent is Ni_3Al phase for both the coatings. When the temperature in the thermal spraying reaches the temperature of 640°C, the reaction between Ni and Al elements will be ignited. This will release a large mount of heat [5], thus the duration of the particle in the high temperature is prolonged and the bonding strength is improved. Without the bond coat the bonding strength of the flame sprayed and plasma sprayed coating reaches 20.4MPa and 29.8MPa, respectively. EDX indicates that the metallic binder phase (gray) forms a continuous network in which the Cr_3C_2 grains (bright) are embedded.

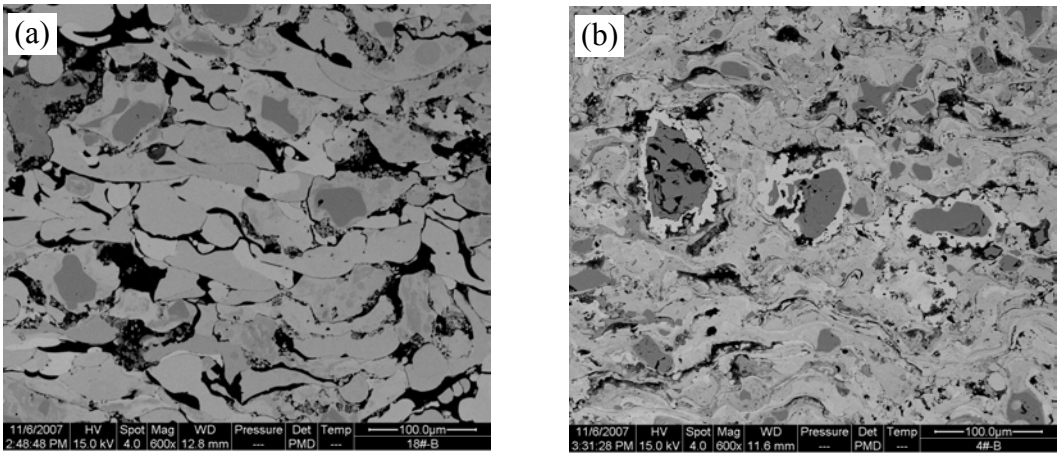

Fig.3 Microstructure of the (a) frame sprayed coating (b) plasma sprayed coating

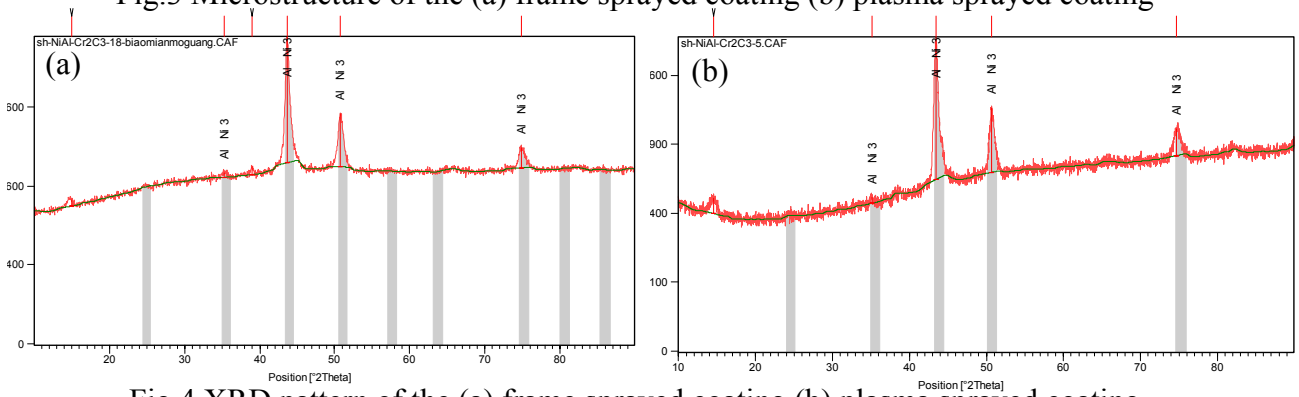

Fig.4 XRD pattern of the (a) frame sprayed coating (b) plasma sprayed coating

Profiles for microhardness versus distance from the coating-substrate interface of the flame and plasma sprayed coatings are given in Fig.5. Both of the coatings have been determined almost the same microhardness, average value of 605 and 610 respectively. The Cr_3C_2 in the coating play a role of particle strengthening [10], thus the microhardness of the coatings is much higher than that of the Ni_3Al coating, which is about 450 HV.

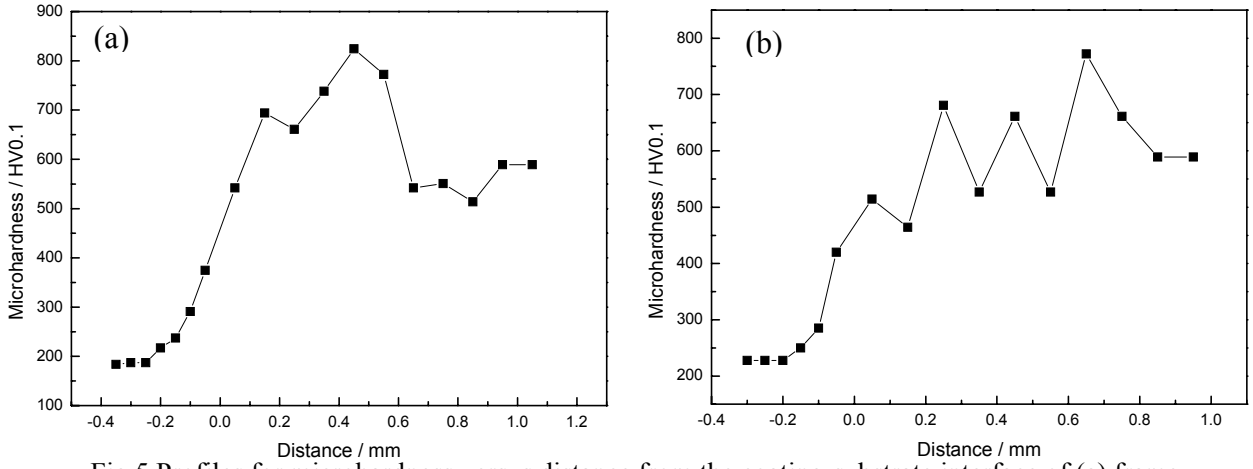

Fig.5 Profiles for microhardness versus distance from the coating-substrate interface of (a) frame sprayed coating (b) plasma sprayed coating

3.3 Friction and wear behavior

The friction and wear values obtained from the evaluated materials of the substrate, flame and plasma sprayed coatings appear in Table 2. The results indicate that all of the three kinds of materials almost have the same friction coefficients, but both the flame and plasma sprayed coating presents better wear resistance performance. The wear resistance of the flame and plasma sprayed coatings is 30% and 120% higher than that of the substrate, which is attributed to the high microhardness of the coatings.

From the surface morphological analyses of the wear scars showed in Fig.6 it is appears that, under the dry friction condition, there is an intensive plastic deformation with marked ploughing grooves in the sliding direction for the substrate. But the flame and plasma sprayed coating only polished traces are observed. At the same time the flame sprayed coating shows spallation under the continuous impact of the wear couple. With the same microhardness the plasma sprayed coating shows better tribological performance than the flame sprayed one. And this is probably for the reason of its compact microstructure, which has better endurance of the impact.

Table 2 Friction and wear behaviour

	Wear out depth (μm)	Wear out width (μm)	Wear out area (μm^2)	Friction coefficient
substrate	129	2720	244160.8	0.82
flame sprayed coating	122.6	2410	184743.7	0.84
plasma sprayed coating	84	2220	110411.7	0.84

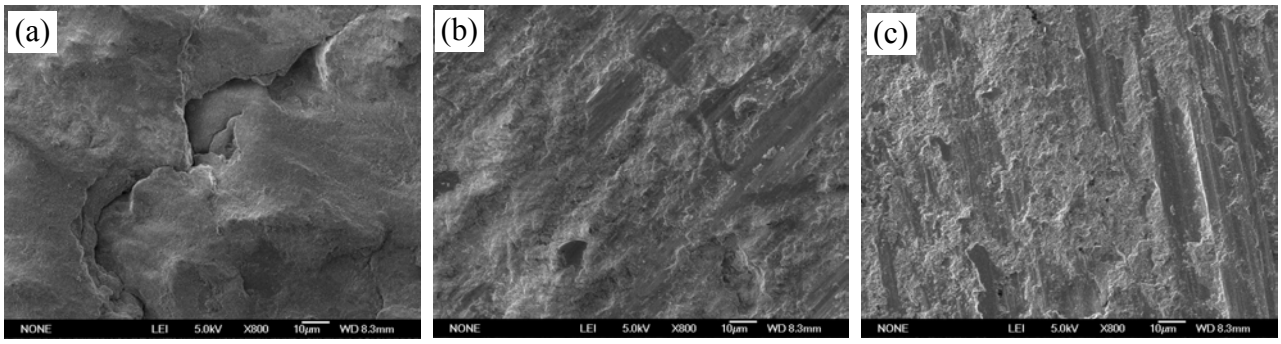

Fig.6 Worn surface of the (a) flame sprayed coating (b) plasma sprayed coating (c) 1045 steel substrate

4. Summary

1) Sprayed Ni-Al-Cr_3C_2 coatings shows better tribological behaviour than 1045 steel under dry friction condition.
2) Of the coatings evaluated, the plasma sprayed coating showed the better performance for its compact microstructure.
3) The morphological studies show the wear mechanism under the dry friction condition is related to plastic deformation and spallation.

References

[1] M.H. Li, Z.Y. Zhang and X.F. Sun: Surface and Coatings Technology Vol. 165 (3) (2003), p. 241

[2] Buta Singh sidhu, D. Puri and S. Prakash: Materials Science and Engineering A Vol. 368 (2004), p.149

[3] Y. Wang, W. Chen and L. Wang: Wear Vol. 254 (2003), p. 350

[4] M.H. Enayati, Z. Sadeghian, M. Salehi and A. Saidi: Materials Science and Engineering A Vol. 375-377 (2004), p. 809

[5] Peiqing La, Mingwu Bai, Qunji Xue and Weimin Liu: Surface and Coatings Technology Vol. 113 (1999), p. 44

[6] H. P. Ng, X. K. Meng and A. H. W. Ngan: Scripta Materialia Vol. 39 (12) (1998), p.1737

[7] C. L. Yeh and W. Y. Sung: Journal of Alloys and Compounds Vol. 384 (2004), p. 181

[8] Y. Wang and W. Chen: Surface and Coatings Technology Vol. 183 (2004), p. 18

[9] T. Sundararajan, S. Kuroda and F. Abe: Corrosion Science Vol. 47 (2005), p.1129

[10] E. Celik, I. A. Sengil and E. Avci: Surface and Coatings Technology Vol. 97 (1997), p.355

Key Engineering Materials 373-374 (2008) pp 19-22

doi:10.4028/www.scientific.net/KEM.373-374.19

Comparative study of 321 stainless steel and 321—Al composite coatings deposited by arc spraying process

Yong-Xiong Chen[1,a], Bin-Shi Xu[1,b], Xiu-Bing Liang[1,c] and Yi Xu[1,d]

[1] National Key Laboratory for Remanufacturing, Academy of Armored Forces Engineering, Beijing 100072, China

[a]famon1599@163.com, [b]xubinshi@vip.sina.com, [c]liangxiubing@yahoo.com.cn, [d]xuyi0226@126.com

Keywords: Arc spray, Composite coating, Stainless steel, Microstructure, Wear property

Abstract. A new type of composite coating (321—Al coating) was prepared by using the 321 austenitic stainless steel wire feed stock as the anode and aluminum wire as the cathode in arc spraying process. In order to compare with the new composite coating, the traditional 321 coating with twin 321 stainless steel wires was fabricated. The microstructure and wear resistance of the coatings were characterized by means of scanning electron microscopy (SEM), X-ray diffraction (XRD), energy dispersion spectroscope (EDS) and MM-200 ring-block type sliding wear tester. Results showed that, except for the aluminum phase addition in the 321—Al coating, no other extra phases produce in comparing with the 321 coating. However, due to the additional aluminum, the 321—Al coating performs quite different microstructure characteristics and tribological behavior. The oxygen content and microhardness of the 321—Al coating are lower than that of the 321 coating, but wear losses are pretty much under the oil lubricated sliding condition. The effect of the microstructure on the wear behavior of the 321—Al coating was also discussed, which is mainly relevant to the characteristic of "ductile aluminum and hard stainless steel composite phases inter-depositing".

Introduction

The single and composite stainless steel coatings prepared by thermal spraying process have perfect wear and corrosion resistant properties, which has been widely studied and applied on repairing or improving the surface properties of mechanical components [1-3]. Illustrationally, the base bearing hole of automobile engine cylinder body is very easy to deform or wear because of the alternating stress and transient shock working status, especially under insufficient oil lubricated conditions. Numerous studies showed that arc spraying 321 stainless steel techniques can remanufacture this kind of automobile engine cylinder body, and had been put in practice in some remanufacturing enterprises [4]. But the coating is very easy to crack owing to the high quenching stress and phase transformation stress during the deposition process, which gives rise to control difficultly the spraying parameters for operation [5]. All those limit the application of arc spraying technique in industry to a large degree. The purpose of this paper is to develop a new technique to prepare 321—Al composite coating by using the 321 stainless steel wire and aluminum wire. The microstructure and mechanical properties of the coating are analyzed as compared with the traditional 321 stainless steel coating.

Experimental Method

The substrate (containing 0.45 % carbon steel plate) was roughened with grit blaster prior to deposition. The coatings were prepared by using the CMD-AS 1620 arc spraying system consisting of a power supply, a wire driver and an arc spraying gun. The 321 stainless steel wire and aluminum wire (99.9% purity) with 2 mm diameter were selected as the spraying feed stocks. As considered that the higher melting point material as the anode and lower melting point material as the cathode can improve the arc stability owing to the relatively balanced melting rates at the two electrode tips [6-8], the wire configuration preparing the 321—Al composite coating was fixed in this paper i.e.

the 321 stainless steel wire is the anode and aluminum wire is the cathode. Spraying parameters used in this research are listed as follows, spray distance of 200 mm, power supply with 32 V and 180 A, atomizing air pressure of 0.6 MPa. To avoid cracking of the arc spraying 321 coating, the intermittent spraying method was selected, which means there is a pause for 15 s within every 30 s spraying time during coating preparation. The continuous spraying method was used for arc spraying 321—Al composite coating.

The samples used for analyzing the coating structure and phase were prepared at first. Then the microstructure and phase composition of coatings were detected by using the QUANT 200 scanning electronic microscope (SEM) equipped with energy dispersive spectroscopy (EDS) and D8 Advance XRD apparatus. A IIMT-3 type microhardness tester was selected to measure coating hardness, more than ten equidistant points from the substrate to the coating surface were tested to every specimen. A WE-10A type material testing machine was used to measure the coating adhesion strength. The column specimens (25 mm diameter) sprayed with coatings and the counterparts roughened with grit blaster were agglutinated together by a type of high bonding strength epoxy adhesive.Wear tests were evaluated by using the MM-200 ring-block type sliding wear tester. The coatings were deposited on the 0.45 % carbon steel block substrates with approximately 500 μm thickness. Then the substrates were milled to the form of the square coupons with dimension 30×30×10 mm^3. The counterpart is a Ti(C, N) ring (hardness= HRA94.5) with diameter of 40 mm and width of 10 mm. The ring was dipped in a 15W/40CD type of lubricant oil. The wear sliding speed was 200 r/min and the load was 150 N. For all tests, the running distance was set for 3000 m. The coefficient of friction (COF) was automatically recorded by computer. Wear width was measured and translated into wear volume, and the structure of the worn surface was examined by SEM.

Results

Microstructure and Composition. Fig. 1 shows the XRD patterns of the 321 and 321—Al coatings. The microstructure of the 321 coating is mainly composed of γ (Fe.Ni), α-Fe, $FeO{\cdot}Cr_2O_3$ and CrO phases. But for the 321—Al coating, except for the Al phase addition, no other alloy phases consisting of Al and compositions of the 321 stainless steel are detected, which manifests that the anode and cathode wire feed stocks was mixed merely with mechanical action during the atomizing process. So the 321—Al coating forms a type of "composite" microstructure.

Fig. 2(a) is the cross-section SEM image of the 321 coating. The coating consists of steel splats labeled as (a) and oxides (b). The steel splats in the coating are very wavy and thin. Except for the above characteristics, micro-cracks (c) and pores (d) in the oxide films are also observed. The formation of micro-cracks confirms that the sprayed 321 stainless steel particles encounter serious distortion and stresses during the deposition process, which leads to the residual stresses concentration in the coating. The oxide films in the coating are hard and brittle and it becomes the weak regions of cracking. The interval spraying process may avoid the macro-cracks expanding to the coating surface, but can not remove micro-cracks initiated from inside of the coating, which will become a potential trouble to post machining and using.

The chemical compositions of the 321 stainless steel coating were further analyzed by EDS. Results show that the mean weight percent of Fe, Cr and Ni elements in the coating is 63.75 %, 16.29 % and 8.28 %, respectively, and the content of oxygen reaches 11.12%.

The SEM image of the 321—Al coating is shown in Fig. 2(b). Similar to the 321 coating, the 321—Al coating is composed with several kinds of splats. But there are some considerable differences between them. EDS analyzing shows that the dark areas labeled as (a) are Al, the light regions (b) are stainless steel, and the dark grey regions (c) mainly contain the oxide of stainless steel and micro-pores (d). According to the results of SEM, XRD and EDS, the microstructure characteristic of the 321—Al coating can be summarized as "inter-deposited by hard steel splats and ductile aluminum splats". Another difference is that the splats of the 321—Al coating are thicker and less wavier than those of the 321 coating. Additionally, a few small stainless steel particles are clad in Al splats as shown in Fig. 2(b).

The EDS analyzing results indicate that the mean content of Al in the whole 321—Al coating is about 36.12 wt%. Due to the addition of Al, the content of Fe, Cr and Ni decreases respectively. Moreover, the content of oxygen in the coating is only 4.07%, which decreases 63% compared with the 321 stainless steel coating.

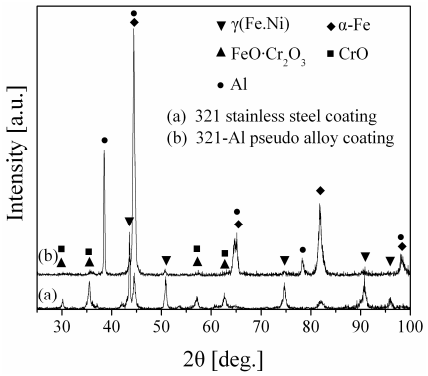

Fig.1 XRD spectra of 321 and 321—Al coating

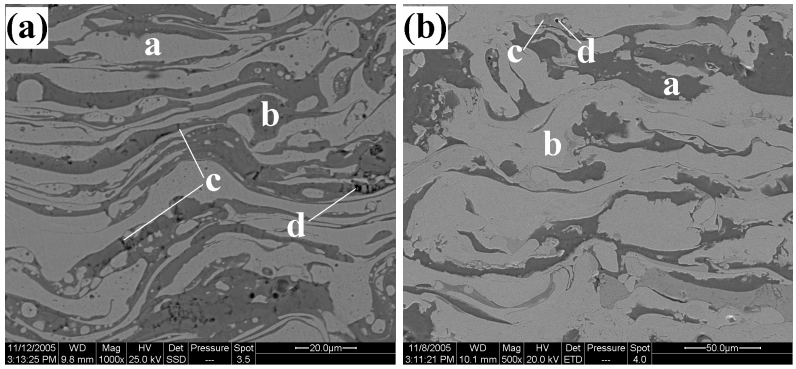

Fig. 2 Cross-section microstructure of 321 (a) and 321—Al (b) coating

Mechanical Properties. The adhesion strengths of the 321 coating and 321—Al coating are pretty much in the same scale, 30±5 Mpa. The mean microhardness of the composite coating is lower than that of the 321 coating, which is helpful to improve its machining property. The distributions along the cross-section of the two coatings are shown in Fig. 3(a). The microhardness value of the 321 coating fluctuates between 360 and 460 HV, while, for the 321—Al coating, it fluctuates more sharply (between 97 and 362 HV). The non-uniform distribution of microhardness reveals the inhomogeneity of coating at microstructure.

Sliding Wear Properties. Fig. 3(b) presents the coefficient of friction and wear losses of the 321and 321—Al coating under wear test condition. The COF of both coatings decreased at the first 250 m sliding distance and then kept a relatively stable value. Although the hardness of the composite coating is lower than that of stainless steel coating, and the COF ranks a higher level, the composite coating exhibits nearly the same wear volume loss as that of the 321 coating. It indicates that the wear resistance mechanism is strongly related with the microstructure of the coating.

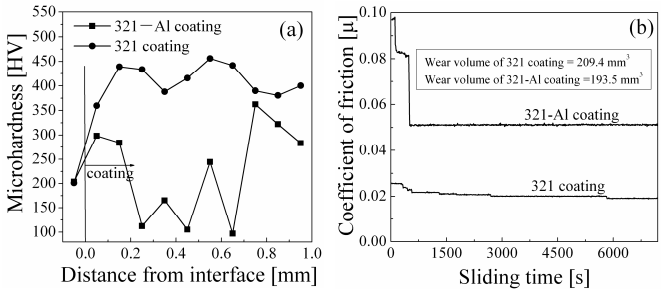

Fig. 3 Microhardness (a) and COF (b) of 321 and 321—Al coatings

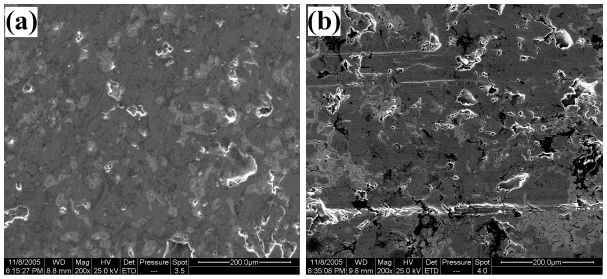

Fig. 4 SEM images of worn surface of 321 (a) and 321—Al (b) coating

Fig. 4 shows the worn surfaces of the 321 coating and 321—Al coating respectively. Different from some bulk metal materials, there are few scratches on the worn surfaces [9], especially for the 321 coating, but merely some scaling pits. The pits of the 321 coating are small and shallow; while for the 321—Al coating, the pits are bigger and deeper.

Discussion

During the atomizing process, the 321 stainless steel particles suffer serious oxidizing and form brittle oxide films. The oxide increases the hardness of coating which is useful to improve wear resistance. But it decreases the cohesive strength between the splats and leads to micro-cracks

initiated from inside of the oxide films.

The 321—Al composite coating has the microstructure characteristic of "ductile and hard phases inter-depositing", which mainly performs two aspects of predominance. Firstly, during the spraying process the Al splats release some stresses resulted from stainless steel splats, and lead to decrease in content of oxide, then decrease the amount of micro-cracks. Secondly, during the wear process the stainless steel splats mainly undertake the part as contacting and polishing with the counterpart, while the Al splats undertake the part as fastening and adhering stainless steel particles, and improves the toughness and shock resistance of the whole coating, thus mitigates the wear. In addition, the microstructure also has the function of impeding the expanding of cracks. Because the hard stainless steel particles inter-distributed in the coating will act on the crack tips to increase energy consumption. When the crack can not get across the stainless particle, the expanding direction will change and tracks will become zigzag, which decreases the rate of cracking.

Summary

Based on the former analyses and discussions, the main conclusions can be summarized as follows:

(1) Similar with the 321 coating, the 321—Al coating prepared by arc spraying technique has typical lamellar structure. But detailed analysis of microstructure discloses some remarkable differences between them. Although the addition of Al in 321—Al coating can not lead to the metallurgic reactions between the anode and cathode feed stocks, a type of "composite" coating with "inter-deposited by hard steel splats and relatively soft Al splats" is formed.

(2) Both of the coating performs a type of exfoliation wear behavior under the oil lubricated sliding condition. The exfoliating pits of 321 stainless steel coating are small and shallow; whereas that of the 321—Al composite coating are relatively bigger and deeper.

(3) Due to addition of Al, the 321—Al coating has lower oxygen content, lower mean microhardness, but performs nearly the same wear volume loss as that of the 321 coating under the lubricated sliding condition. The microstructure of the 321—Al composite coating with "ductile + hard phases inter-depositing" characteristic has such advantages as releasing the residual stress, improving the shock resistance and impeding the outspread of cracks, thus mitigates the wear process.

Acknowledgements

The authors are grateful to the priority support by China Natural Science Foundation (50735006), and the National "973" Project of China (2007CB607601).

References

[1] J.F. San, Z. Du and Z.F. Bi: Tribology Vol. 18 (1998), p. 119. (in Chinese)

[2] A.A. Syed, A. Denoirjean, P. Fauchais and J.C. Labbe: Surf. Coat. Technol. Vol. 200 (2006), p. 4368

[3] L.Z. Du, B.S. Xu and S.Y. Dong: Trans Nonferrous Met Soc China Vol. 14 (2004), p. 370

[4] Z. Xing, A.L. Jiang and J.J Xie: Surface Engineering of China Vol. 17 (2004), p.1. (in Chinese)

[5] J. Matejicek and S. Sampath: Acta Materialia Vol. 51 (2003), p. 863

[6] H. Aqeorqes and P. Fauchais: Thin Solid Films Vol. 370 (2000), p. 213

[7] H.L. Liao, Y.L. Zhu and T.R. Bolota: Surf. Coat. Technol. Vol. 200 (2005), p. 2123

[8] T. Watanabe, T. Sato and A. Nezu: Thin Solid Films Vol. 407 (2002), p. 98

[9] L. Prchlik and S. Sampath: Wear (2006), in press.

Key Engineering Materials 373-374 (2008) pp 23-26

doi:10.4028/www.scientific.net/KEM.373-374.23

Effect of HVOF sprayed MCrAlY coating on thermomechanical and isothermal fatigue life of superalloy M963

Z.W. Huang[1, 2, *], Z.G. Wang[2, a], S.J. Zhu[3, b], F.H. Yuan[2, c], F.G. Wang[1, d]

[1] School of Materials Engineering, Dalian University of Technology, Dalian, China

[2] Shenyang National Laboratory for Materials Science, Institute of Metal Research, Chinese Academy of Sciences, Shenyang 110016, China

[3] Department of Intelligent Mechanical Engineering, Fukuoka Institute of Technology, Fukuoka, Japan

[*] Corresponding author, zhwhuang@imr.ac.cn, [a]zhgwang@imr.ac.cn, [b]zhu@fit.ac.jp, [c]fhyuan@imr.ac.cn, [d]fgwang@dlut.edu.cn

Keywords: Thermomechanical fatigue; Isothermal fatigue; Superalloy; MCrAlY coating; HVOF

Abstract

A cast nickel based superalloy M963 was coated by high-velocity oxy-fuel (HVOF) spraying process. The effect of HVOF MCrAlY coating on thermo-mechanical fatigue (TMF) and isothermal fatigue (IF) in M963 was studied to understand fatigue life and failure mechanisms in coated and uncoated M963 alloy. Two types of TMF tests, i.e. in-phase (IP) and out-of-phase (OP), were performed in temperature range of 450~900°C, and IF tests were conducted at 900°C. It was found that the coating had a detrimental effect on fatigue life under OP TMF, while a beneficial effect of the coating existed under IP TMF and IF. Crack initiation time in the coated specimen was shorter than that in the uncoated specimen and the former's crack density was higher than the latter's one under OP TMF. The relationship of deformation and fracture response with fatigue life was discussed based on microscopic analysis.

Introduction

MCrAlY overlay coatings have been widely used in industrial gas turbines to provide good oxidation resistance, corrosion resistance and preserve good mechanical properties of nickel-based superalloys at elevated temperature [1]. Generally, MCrAlY coatings are produced by vacuum plasma spraying (VPS) technique. However, the VPS technique is expensive in use, interests have been paid to find a technological alternative [2]. Recently, a new thermal spraying process—high-velocity oxy-fuel (HVOF)—was developed and used to produce MCrAlY coatings. HVOF sprayed coatings have very low porosity, high hardness, good wear resistance and a strong ability to resist high-temperature corrosion [3]. The oxidation behavior and the bond strength of HVOF sprayed coatings have been investigated intensively [4,5], however, little research has been done about the effect of the coating on fatigue life.

In the present study, the results of investigation on the influence of HVOF sprayed coating on the thermomechanical and isothermal fatigue life of a cast nickel-based superalloy M963 were presented. In particular, the effect of the phasing of strain and temperature, such as in-phase and out-of-phase, on the failure mechanisms of the coated superalloy was investigated.

Materials and Experiments

The material employed in this study was a cast nickel-base superalloy M963 with a chemical composition in wt pct of 0.15 C, 8.89 Cr, 6.00 Al, 2.55 Ti, 1.64 Mo, 10.1 W, 10.0 Co, 1.10 Nb, 0.03 Zr, 0.03 B, 0.02 Ce, 0.01 Y, balance Ni. The master alloy was remelted and cast into test bars of 16mm in diameter. Before machining, the bars were solution treated at 1210°C for 4h and followed by air-cooling. Cylindrical specimens with a gauge diameter of 6mm and a gauge length of 25mm

were taken from the bars for both TMF and IF tests. A NiCrAlY (Ni-25Cr-5Al-0.5Y) alloy was deposited on the gauge section of the superalloy with a thickness of ~150μ m by the HVOF spraying process. The cross-section of the coated specimen in as-sprayed state showed a dense and uniform coating layer, as shown in Fig.1.

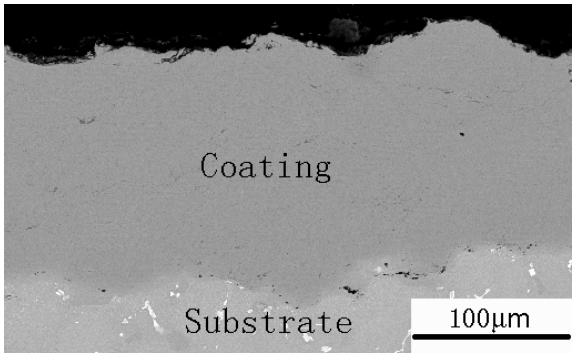

Fig. 1. SEM photograph showing cross-section of MCrAlY coated M963 specimen.

Fatigue tests were conducted on an MTS810 servo-hydraulic thermomechanical fatigue machine on specimens both uncoated and coated with computer control. A high-frequency induction generator was used for heating. Cooling was mainly achieved by thermal conduction into the specimen grips and could be forced by blowing compressed air. The temperature was measured and controlled with a thermocouple spot-welded in the middle of the gauge length. The total strain was measured using a high temperature axial extensometer of 16mm gage length with ceramic rods. A triangle waveform was used for both thermal cycling and mechanical cycling.Two typical modes of TMF, i.e. IP (maximum tensile mechanical strain occurs at maximum temperature) and OP (maximum tensile mechanical strain occurs at minimum temperature) were carried out in temperature range of 450~900℃. Additionally, isothermal fatigue tests were conducted at a constant temperature of 900°C. All tests were performed at two mechanical strain (ε_{mech}) amplitudes i.e. 0.50% and 0.35% at a strain rate of $1\times10^{-4}s^{-1}$under mechanical strain control.

Results and Discussions

Fatigue test results for uncoated and coated M963 are summarized in Fig. 2 for IP TMF, OP TMF and IF cases. It can be seen that there is a lifetime reduction for coated specimens under OP TMF loading, whereas the lifetime in the coated specimens is longer than that in the uncoated specimens under IP TMF and IF loadings. IF lifetime is longest and OP TMF lifetime is shortest.

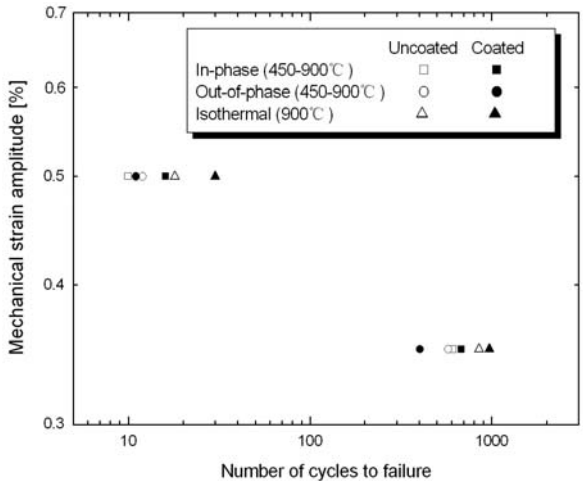

Fig. 2. Effect of MCrAlY coating on TMF and isothermal fatigue life in M963 alloy.

SEM observation of longitudinal cross-sections close to fracture surface shows that crack initiates at rough surfaces in the coated specimens, as shown in Fig. 3a and is deflected into the interface between the coating and the substrate and finally propagates into the substrate (Fig. 3b). The number of cracks initiated on the coating surface is the most under IF and the least under IP TMF. The crack propagation in the substrate is in a mixed transdendritic and interdendritic manner, in which interdendritic cracking dominates under IP TMF conditions (Fig. 3c). This is because the crack is open at elevated temperature and the crack tip is exposed to air, while interdendritic regions which are rich in easily oxidized elements such as aluminium, titanium, chromium, etc. provide rapid propagation channels for the crack. Moreover, residual grit particles embedded in the surface of the substrate during abrasive blasting may promote crack initiation and propagation, as shown in Fig. 3b and Fig. 4, which are alumina identified by EDS and EPMA. These irregular-shaped alumina particles can act as stress concentration sites during fatigue process, and it can be expected that longer fatigue life would be obtained if the particles could be properly removed before fatigue tests.

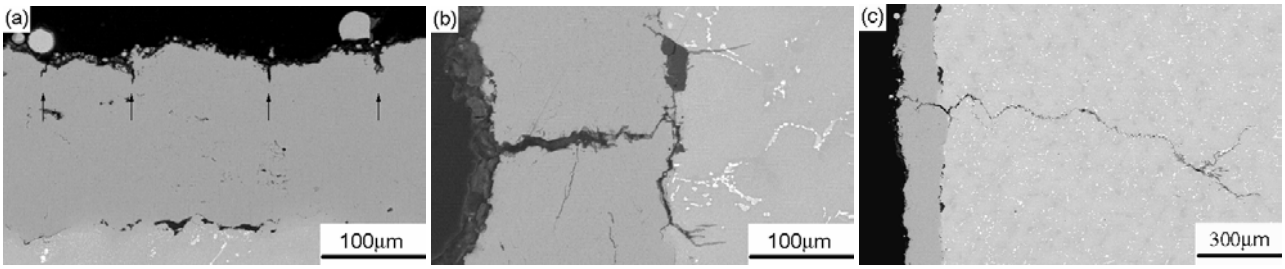

Fig. 3. SEM photographs showing fatigue cracks on cross-sections of MCrAlY coated M963: (a) Isothermal fatigue, $\Delta \varepsilon_{mech}/2=0.35\%$; (b) OP TMF, $\Delta \varepsilon_{mech}/2=0.35\%$; (c) IP TMF, $\Delta \varepsilon_{mech}/2=0.35\%$. Arrows indicate cracks initiated at rough surface.

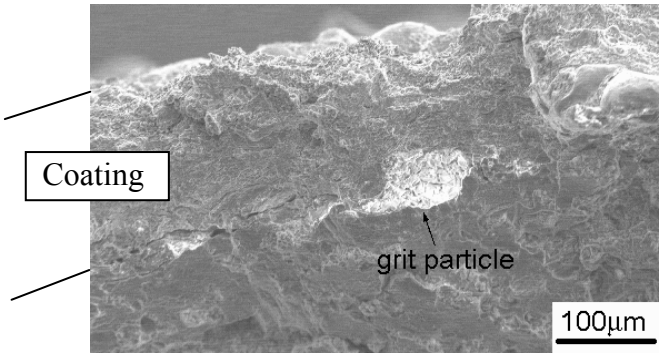

Fig. 4. SEM photograph showing fracture appearance of in-phase TMF ($\Delta \varepsilon_{mech}/2=0.35\%$) in MCrAlY coated M963.

Since the cracking of coating strongly influence the failure of coated specimen under OP TMF, a quantitative analysis of the cracking behavior of the coated superalloy under OP TMF was performed and compared with that of the uncoated superalloy, as shown in Fig.5. Tests were stopped after a defined number of cycles and the crack density in substrate was determined by SEM. It can be seen that no crack in the uncoated substrate was observed after fifty cycles; in contrast, a few cracks were observed in the case of coated superalloy. This observation clearly shows that early cracking of coating under OP TMF will accelerate the initiation process in superalloy and lead to a reduced fatigue life.

The different cracking behaviors of MCrAlY coating under IP, OP TMF and IF may be attributed to the transition of the coating's mechanical behavior as a function of temperature. Fine-grained MCrAlY coating shows ductile deformation behavior and low strength at high temperatures and brittle behavior and high strength below a certain temperature (called ductile-to-brittle transition

temperature, DBTT). The DBTT of MCrAlY coating materials is usually around 650℃ [6]. Under OP TMF loading, the coating is in tension at low temperatures, therefore early cracking of the coating occurred. In IP TMF loading, the coating is ductile enough to prevent cracking due to the coating is in tension at high temperatures. As a result, few cracks in coating are observed in IP TMF tests. However, in the case of IF condition at 900℃, both tension and compression are at high temperature. As a result, the coating layer is like a

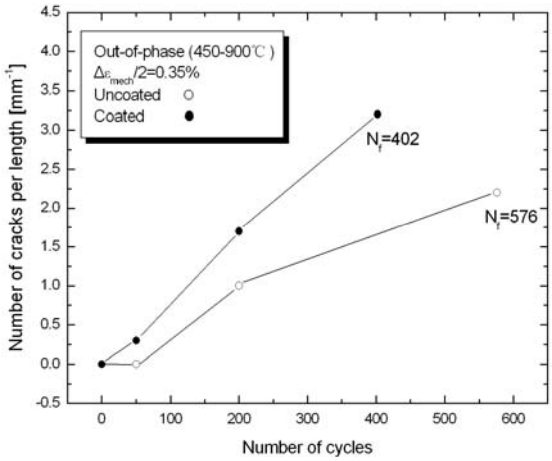

Fig. 5. Micro-crack density in M963 substrate versus number of cycles in OP TMF for $\Delta\varepsilon_{mech}/2=0.35\%$.

ductile metal and a lot of small surface cracks initiate by cyclic plastic deformation at high temperature. However, such kind of small cracks would not decrease the fatigue life of the coated specimen due to the blunting effect of the ductile coating on crack tip at 900℃. The coating can still preserve its good oxidation resistance for the superalloy, thus a longer fatigue life was obtained in the coated specimens in both IF and IP TMF tests.

Summary

Effect of high-velocity oxy-fuel spray coatings on thermomechanical and isothermal fatigue life of superalloy M963 was investigated. Detrimental effect of coating on fatigue life was observed in OP TMF condition, while in the case of IP TMF and IF conditions, beneficial effect of the coating on fatigue life was obtained. Crack initiates at rough surfaces in the coated specimens and deflects into the interface between the coating and the substrate and finally propagates into the substrate. The number of cracks initiated on the coating surface is the most under IF and the least under IP TMF. The early cracking of coating under OP TMF leads to a reduced fatigue life.

References

[1] R. Mevrel: Mater. Sci. Eng. A 120 (1989), p. 13

[2] W. Brandl, D. Toma and H.J. Grabke: Surf. Coat. Tech. Vol. 108-109 (1998), p. 10

[3] T.S. Sidhu, R.D. Agrawal and S. Prakash: Surf. Coat. Tech. Vol. 198 (2005), p. 441

[4] F. Tang, L. Ajdelsztajn, G.E. Kim, V. Provenzano and J.M. Schoenung: Surf. Coat. Tech. Vol. 185 (2004), p. 228

[5] Y.Y. Wang, C.J. Li and A. Ohmori: Surf. Coat. Tech. Vol. 200 (2006), p. 2923

[6] R. Kowalewski and H. Mughrabi: Mater. Sci. Eng. A 247 (1998), p. 295

Key Engineering Materials 373-374 (2008) pp 27-30

doi:10.4028/www.scientific.net/KEM.373-374.27

Performance Study of Erosion Wear of Nanostructured WC-12Co Coatings Sprayed by HVOF

Z. X. Ding[1,a], Q. Wang[2,b], Z. L. Liu[1,c]

[1]Wuhan University of Technology, Wuhan 430063, China

[2]Hunan University, Changsha 410082, China

[a]email: zxding@whut.edu.cn, [b]email: wangqun72@163.com, [c]email: zlliu812@163.com

Keywords: Erosion wear; nanostructured WC-12Co coatings; HVOF; coating microstructure

Abstract. In the paper, nanostructured, multimodal and conventional WC-12Co cermet coatings were sprayed by HVOF and the properties and structures of the coatings such as microhardness, microstructure, phase composition were compared. Finally sand solid and slurry erosion wear tests were carried out and their wear failure mechanisms were explored by XRD and SEM analysis. Research results show that microstructures of nanostructured and multimodal WC-12Co coatings prepared by HVOF are dense with little porosity, and their microhardness values are obviously higher than conventional WC-12Co coating. As well, it was found that nanostructured and multimodal WC-12Co coatings exhibited better sand solid and slurry erosion wear resistance in comparison with conventional coating and nanostructured WC-12Co coatings possessed the best sand solid erosion resistance properties at large impact angles and slurry erosion wear resistance. Testing results also show that although decarburization of WC occurred during spraying multimodal and nanostructured WC-12Co powders, the decarburization of WC for the nanostructured powder was more severe.

Introduction

Erosion is a main failure mode of materials and equipment and exists in many industrial fields, such as aerospace, mechanism, metallurgy, energy sources, chemical industry. Thermal sprayed WC-Co cermet coatings have been used widely in these industries because of the coatings' excellent erosion wear resistance. Research shows that the hardness and strength of WC-Co materials increase as the WC particle size reduces; In comparison with conventional WC-Co cermet, nanostructured WC-Co materials possess higher hardness and toughness, more excellent sliding wear resistance and more extensive application potential[1~2]. In thermal spraying, the nanostructured WC particles are more susceptible to decarburization because of the finer size and higher surface to volume ratio of the WC particles. Since high velocity oxy-fuel (HVOF) spraying possesses the features of high flame velocity, low flame temperature, residence time of the WC particles can be shortened and the WC decarburization can decrease during HVOF spraying for WC-Co feedstock powder. Therefore HVOF process is more suitable to deposit nanostructured WC-Co coatings than other thermal spraying processes [3~4].

In the paper, nanostructured, multimodal and conventional WC-12Co cermet coatings were deposited by HVOF and the properties and structures of the coatings such as microhardness, microstructure, phase composition and erosion resistance were compared. Finally the failure mechanisms of the WC-12Co coatings erosion wear were explored.

Experimental procedure

Materials and coating fabrication. Nanostructured, multimodal and conventional WC-12Co powders were used as feedstock in the study and they were marked N1, M1 and C1. Nanostructured and multimodal WC-12Co powders respectively were Infralloy S7412 and Nanomyte M1. They

were produced by an agglomeration method and micro-nanosized particle ratio is 70/30 in M1. Conventional WC-12Co powder was produced by sintering and crushing method, the particle size is 10~45μm. The substrate materials is Q235 mild steel for coating samples, the dimensions are 80×60×3 mm for solid sand erosion test and φ 20×25 mm for slurry erosion wear test. Prior to spray the substrate samples were degreased and grit blasted with 60 mesh Al_2O_3. About 0.45 mm thick WC-12Co was coated using $T_{I\text{-}II\ 3200CY}$ HVOF system and kerosene was used as fuel.

Experiment methods. The micrographs of WC-12Co coating worn surfaces, the microstructures of typical "as-sprayed" coatings were analyzed with S-570 scanning election microscope (SEM). Phase analysis of the starting powders and coatings was performed by D5000 XRD and the coating microhardness was measured with 71 model micro Vickers using a load of 200 g. In the solid sand erosion wear tests, 80~120 mesh Al_2O_3 erodent was used and other testing parameters were: 0.5 MPa air pressure, 120 mm erosion distance, 8.0 mm nozzle diameter, 30° and 90° impact angle, 3 min and 2 min erosion duration respectively for 30° and 90° impact, 20 g/s particle feedrate. In slurry erosion wear tests, the slurry consisted of 86% 20~40 mesh river sand and 14% water. Rotational speed of blade wheel is 595 r/min and linear velocity of sample is 9.8 m/s. Impact angle of wear surface is 30° and the erosion duration was for 6 hours. The weight loss of the samples was measured using TG328 electric balance, accurate to 0.1 mg.

Results and Discussion

Microstructure of WC-12Co coatings. The surface morphology of nanostructured, multimodal and conventional WC-12Co coatings by HVOF are presented in Fig. 1, and Fig. 2 shows the coatings' cross-sectional microstructures. In C1 coating, unmolten, coarse shape WC particles can be observed and this demonstrates that only surface of micron size WC-Co particles melt, but WC still was in solid state. In M1 coating, nanosized WC-12Co materials were heated and melt, but quite a lot of micron size WC-12Co particles were in semi- molten state. In N1 coating, the most of WC particles were heated up to melt because of the finer size, higher surface to volume ratio and activity. It can be observed in Fig. 2 that in the three kinds of coatings by HVOF the porosity is very low, the microstructure is dense and the interlamellar cohesion is strong, but N1 coating possesses the lowest porosity and the densest microstructure.

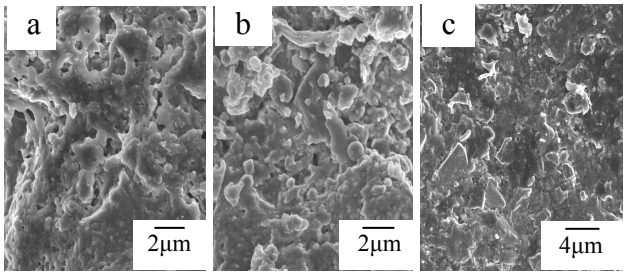

Fig. 1 Surface micrographs of WC-12Co coatings (a: N1 coating, b: M1 coating, c: C1 coating)

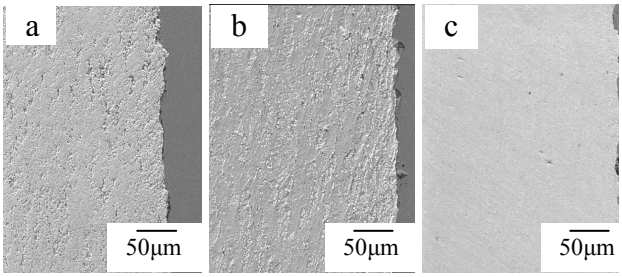

Fig. 2 Micrographs of WC-12Co coatings (a: C1 coating, b: M1 coating, c: N1 coating)

Phase composition of WC-12Co powders and coatings. Fig. 3 shows the XRD analysis of WC-12Co powders and coatings produced by HVOF. The XRD study of the initial phases of N1, M1 and C1 powders showed no differences and the typical XRD pattern is presented in Fig. 3. They were pure WC and Co. In C1 coatings, the phase compositions are almost the same as those of starting powder, consisting mainly of WC and Co. In M1 and N1 coatings, the coatings are composed of WC, W_2C, W and Co_6W_6C crystalline phases. The phases of W_2C, W and Co_6W_6C have been generated during the spraying processes. Meanwhile an amorphous/nanocrystalline zone exists at 2θ angles between 35° and 48° for M1 and N1 coatings. Though M1 and N1 both powders suffered the typical decarburization during the spraying, the nanostructured WC-12Co powder had a greater decarburization as showed in Fig. 3. It can be concluded that the decarburization would be